INVESTIGATING HOST RESPONSE TO VIRAL INFECTION THROUGH PROTEOMICS: A STUDY OF MURINE NOROVIRUS

by

Linnzi Marie Furman

A thesis submitted in partial fulfillment
of the requirements for the degree

of

Master of Science

in

Biochemistry

MONTANA STATE UNIVERSITY
Bozeman, Montana

April 2008

APPROVAL

of a thesis submitted by

Linnzi Marie Furman

This thesis has been read by each member of the thesis committee and has been found to be satisfactory regarding content, English usage, format, citation, bibliographic style, and consistency, and is ready for submission to the Division of Graduate Education.

Dr. Brian Bothner

Approved for the Department of Chemistry and Biochemistry

Dr. David Single

Approved for the Division of Graduate Education

Dr. Carl A. Fox

STATEMENT OF PERMISSION TO USE

In presenting this thesis in partial fulfillment of the requirements for a master's degree at Montana State University, I agree that the Library shall make it available to borrowers under rules of the Library.

If I have indicated my intention to copyright this thesis by including a copyright notice page, copying is allowable only for scholarly purposes, consistent with "fair use" as prescribed in the U.S. Copyright Law. Requests for permission for extended quotation from or reproduction of this thesis in whole or in parts may be granted only by the copyright holder.

Linnzi Marie Furman

April 2008

TABLE OF CONTENTS

TABLE OF CONTENTS - CONTINUED

LIST OF TABLES

Table Page

LIST OF FIGURES

LIST OF FIGURES - CONTINUED

GLOSSARY OF ABREVIATIONS

FBS – Fetal Bovine Serum

DMSO – dimethyl sulfoxide

MNV – Murine Norovirus

FCV – Feline Calicivirus

h.p.i. – hours post infection

FLICA – fluorescently labeled inhibitor of caspases

PI – propidium iodide

ABPP – Activity based protein profiling

2D-DIGE – Two-dimensional differential gel electrophoresis

PFU – plaque forming units

DMEM – Dulbecco's Modified Eagle's Medium

PCD – programmed cell death

DTT – dithiothreitol

SDS-PAGE – sodium dodecyl sulfate polyacrylamide gel electrophoresis

ROS – reactive oxygen species

STAT1 – signal transducer and activator of transcription

ABSTRACT

Norovirus causes roughly 23 million cases of foodborne illnesses in the United States each year. While this virus was characterized over 30 years ago, it remains non-cultivatable in human cells, resulting in an incomplete understanding of the host cell's response to infection. However, in 2004 murine norovirus (MNV) was found to be cultivatable in mice and has since been successfully cultured in RAW 264.7 cells. MNV has become an important model system for studying norovirus, as it is structurally and genetically similar to human norovirus. A global proteomics approach using fluorescently tagged, activity-based probes and 2D differential gel electrophoresis analysis was used to study MNV infection. Specifically, the process of cell death was investigated to determine if apoptosis, or programmed cell death, occurred in response to infection. Through the 2D differential gel analysis, 27 differentially regulated proteins were identified at 4 hours post infection, and 22 differentially regulated proteins were identified at 12 hours post infection; a strong majority of these proteins have been related to apoptosis in the literature. Using fluorescently-labeled activity-based probes and fluorimetric assays, we have monitored the activation of several caspases induced by viral infection. Infected samples show a significant increase in caspase activity over control samples within the first few hours post infection, indicating a virally induced activation of caspases. Cells were also infected in the presence of a pan-caspase inhibitor, Boc-D(OMe)-fmk, which led to caspase-independent cell death. Using propidium iodide and Hoechst staining, it was concluded that infected cells undergo necrosis in the presence of the caspase-inhibitor, while those infected in the absence of the inhibitor undergo apoptosis. From these studies it can be concluded that cells infected with MNV undergo a caspase-mediated, apoptotic cell death, while the caspase-independent cell death can be classified as necrosis. This study provides significant insight to norovirus-induced cell death.

INTRODUCTION

Norovirus

Noroviruses are the leading cause of non-bacterial gastroenteritis, commonly referred to as the stomach flu, and cause roughly 23 million cases of foodborne illness annually in the United States alone (CDC, 1999). The virus infects people of all ages and is highly contagious amongst those susceptible to infection. The illness is most commonly known for its fast-spreading outbreaks on cruise ships, college campuses, military bases, and in nursing homes, restaurants, and other semi-closed communities [1]. Symptoms become present twelve to 48 hours post-infection and usually last for 24 to 60 hours. While the majority of those infected with the virus recover in one to three days with no long-term side effects, roughly 50,000 cases in the U.S. result in hospitalization annually and approximately 300 of those cases become fatal (CDC, 1999).

Noroviruses, previously referred to as Norwalk-like viruses or small round-structured viruses, are a group of forty genetically heterogeneous viruses that belong to the family *Caliciviridae*. There are seven norovirus genogroups (G), GI through GVII, of which GI and GII are known to infect humans while the other genogroups infect cattle, swine, and mice[2]. GI includes the Norwalk, Desert Shield, Southampton, and Chiba-like virus strains, which are less prevalent than the GII strains, which include the Hawaii, Snow Mountain, Lordsdale, and Bristol-like viruses. Both strains can be passed directly from person-to-person through an oral-fecal route or through the environment.

Noroviruses are quite variable, with capsid protein amino acid sequence variation of up to 40 percent within a genogroup. Between genogroups, sequence variation can be greater than 50 percent[3].

Noroviruses are positive-sense, single-stranded, RNA viruses with a 7.7 kb genome. They are a non-enveloped, T=3, icosahedral virus, and are roughly 30 nanometers in diameter [1] (Figure 1). They are the only group of animal viruses known to date whose capsid consists of a single protein [4]. Their genomes contain three open reading frames (ORFs). ORF1 consists of non-structural proteins: p48, NTPase, p22, VPg, Pro, and RdRp. ORF2 encodes the capsid protein, VP1, while ORF3 codes for VP2, a structural protein that may act as scaffolding for VP1, or as a structural intermediate complex between VP1 and RNA. Norovirus RNA has a 5' genome-linked VPg protein and has a 3' poly$(A)_n$ tail [5]. The non-structural proteins consist of a 3C-like protease, which is responsible for cleaving the nonstructural ORF1 polyprotein during and after translation [6], an RNA-dependent RNA-polymerase, and others.

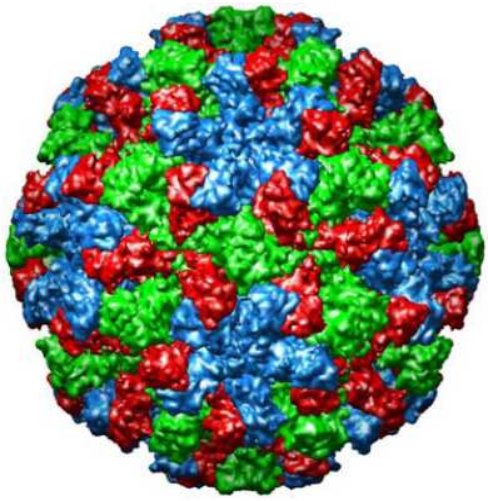

Figure 1. A reconstructed crystal structure of norovirus from VIPERdb Virus Particle Explorer. Noroviruses are a T=3 icosahedral virus with 180 subunits.

In 2005, Hardy summarized the structure and function of the known norovirus proteins[4]. VP1 is of considerable interest, as it is the major capsid protein and thus plays an important role in viral infection and entry into a host cell. This 60kDa protein consists of two conserved domains. VP1 has two distinct regions; one region is termed the S, for shell, while the other is termed P, for protruding domain. The P domain has two sub-domains, P1 and P2. P2 is the region within the P1 amino acid sequence that extends furthest from the shell domain, and is the region of high variability most likely associated with receptor binding. Both regions of VP1 are highly variable and are correlated with strain specificity. The S domain has 30 percent sequence identity between strains, while the P1 and P2 domains are only about 10 percent identical between strains [7].

The VP1 structural protein has been shown to auto-assemble into VLPs when expressed in a recombinant baculovirus or in yeast cells, making it the focus of many studies, as it is structurally and antigenically identical to infectious virions [4,8]. It should be noted that there has been some controversy regarding the importance of VP2 in structural stability. VP2 is a much smaller protein (29kDa) that is not well characterized. It has been suggested that it is involved in RNA packaging or binding, due to a very basic N terminus. A study in 2003 indicated that the presence of VP2 stabilizes the capsid cage formed by VP1 [9], suggesting it may also play an important role in virus assembly and stability.

Nonstructural norovirus proteins have yet to be fully characterized, although some of the details are known. Protein p48 may provide scaffolding for the assembly of a replication complex [10], although this has yet to be confirmed. Protein p22 may be related to the 3A protein of picornavirus genomes, as it is located in the equivalent genome

location [11]; however, overall sequence similarity is weak. VPg has been found in the murine norovirus, and it also exists in the human noroviruses [5]. VPg covalently likes to genomic and subgenomic mRNAs and is involved in protein translation initiation. Two of the norovirus proteins have homologues in picornaviruses: a 3C protease with a chymotrypsin-like fold and an RNA-dependent RNA polymerase [12].

The most common way to examine the binding interactions between norovirus and cells is to create virus-like particles, which are self-assembled VP1 cages created from a recombinant baculovirus expressed in insect cells. VLPs are virtually indistinguishable from infectious virions, which make them a very useful tool. This was first reported in 1990 by Jiang et al. [13]. Prior to the generation of VLPs from recombinant baculovirus, most research was performed on virions extracted from stool samples of individuals infected with norovirus. VLPs have been used extensively in the last ten years to investigate the details of norovirus receptor binding, and this alone has significantly advanced the research on noroviruses. Recent advances in understanding viral binding have led to an effort to develop protein capsid vaccines against norovirus [8,14-17], and at least one vaccine is under Phase I clinical trials (Ligocyte Pharmacueticals Inc.).

Although norovirus was identified in the early 1970s, little is known about its replication and life-cycle [16]. Unfortunately, attempts to grow human norovirus in cell culture have been unsuccessful[18]. In the mid-1990s norovirus attachment and entry were addressed. In 1996, it was found that of thirteen different cell lines, Norwalk VLPs showed a tropism for human intestine cells, or differentiated Caco-2 cells [19]. Recently, Karst et al. were able to study the closely related murine norovirus (MNV-1), which has become a model virus for studying human norovirus. This study showed that STAT1

plays a critical role in innate immunity to norovirus, as MNV infection in STAT1 deficient mice is lethal[20]. In 2004 Wobus et al. reported that MNV-1 has a tropism for dendritic cells and macrophages; this was the first report of a successful cell culture system to study noroviruses. They suggested that the dendritic cells may provide the transportation for the virus to enter the subepithelial cells in the intestine, which aids the norovirus progression [21]. Since the discovery of this model system, only a handful of papers have been published regarding murine norovirus.

Of the 25 papers published on MNV, five of these are related to virus stability. It has been shown that MNV is relatively stable in acidic and basic environments, under extreme temperatures, and at a large range of pH values [22-24]; it is especially stable when compared to the feline calicivirus [22]. Two studies revealed that MNV can be successfully inactivated with UV [25] and under high pressure [26]. The remaining articles vary in topic from isolating novel forms of the virus from laboratory mice [3,27,28] to further characterization of the viral proteins [5,14,29].

Apoptosis

One way cells respond to viral infection is through apoptosis or apoptosis-like programmed cell death. Recent review articles on apoptosis suggest that there are many types of programmed cell death (PCD), and that while apoptosis is well characterized, these intermediate forms of PCD are not as fully understood. Apoptosis is defined by a set of molecular characteristics, including chromatin condensation from DNA fragmentation [30], cell shrinkage[31], membrane blebbing [32], phosphatidylserine exposure [33], and caspase activation [34]. Cells may undergo apoptosis-like PCD if they exhibit many of

the characteristics of traditional apoptosis but lack the signature chromatin condensation of true apoptosis. A third characterization of PCD is deemed necrosis-like PCD, which again lacks the chromatin condensation, but unlike traditional necrosis, cells death is programmed due to the activation of some cell signaling pathways [35]. Necrosis is simply non-programmed cell death, which occurs when cells dies due to physical parameters. While apoptosis is the best characterized mode of PCD, there are still many questions regarding the multiple signaling pathways that induce this complex process.

Viruses have been shown to both inhibit and induce apoptosis, and the advantages of each are still being investigated [35-37]. In some circumstances, apoptosis results in apoptotic bodies, or small membrane-bound bodies, which allow the virus to be ingested through phagocytosis and thereby go undetected by neighboring cells. This is clearly advantageous, as the virus is allowed to spread directly from cell to cell without being excreted into the extra-cellular matrix. This is just one example of how a virus can use apoptosis to its advantage. A 2002 review article of apoptosis and viruses lists over a dozen viruses that have been documented to induce apoptosis during infection, each with its own mechanism for activation, and there are even more viruses that are known to inhibit apoptosis [35].

The mechanisms for inhibiting apoptosis target a handful of proteins, including caspases, Bcl-2, TNF (tumor necrosis factor), NFκB, PKR (dsRNA-dependent protein kinase), p53, and the oxidative stress pathway. Both NFκB and PKR stimulate interferons (IFNs), which are critical to the host's defense against viral infection. Most of the mechanisms that inhibit apoptosis through Bcl-2, TNF, p53 and NFκB ultimately led to the prevention of caspase activation; these proteins indirectly activate the initiator

caspases 8 and 9, which activate caspase-3, leading to DNA fragmentation and apoptosis; by blocking any one of these proteins upstream of the initiator caspases, a virus can stop apoptosis.

While the connection between infection and apoptosis is well described for a number of viruses, for others this has yet to be investigated. Apoptosis as a feature of calicivirus infection is not well characterized. It has been shown that apoptosis can occur in cells infected with feline calicivirus, as determined by an increase in caspase-3 activity [38]. It has also been suggested that caspase-3 could potentially cleave the norovirus polyprotein, which would suggest that apoptosis is required for viral replication[39]. This study correlated an increase in caspase-3 with the cleavage of the viral polyprotein, and two regions on the polyprotein were mapped as potential cleavage sites. While apoptosis in norovirus-infected cells has not been confirmed, an increase in caspase-3 activity would strongly suggest that apoptotic processes are initiated by infection.

Proteomics

Traditional experiments designed to follow viral infection at the proteomic level use techniques that target individual proteins, such as western blots or fluorescently-labeled antibodies for imaging. These experiments are limited by the fact that they only report on specific proteins that are selected for observation. Host-cell responses to viral infections often activate multiple pathways as defense from the intruder. A global perspective on protein changes in the cell during infection allows greater insight to the complexities of viral infection.

Over the past decade, techniques for two-dimensional differential gel electrophoresis (2D-DIGE) have become a powerful approach for the global study of cellular proteins. In the past several decades, techniques incorporating 2-D polyacrylamide gel electrophoresis (2D-PAGE) and mass spectrometry have become a routine method for the rapid identification of proteins. Unfortunately, quantitative protein abundance comparisons were limited. Limitations were due to a lack of sensitivity (Coomassie), lack of dynamic range (silver staining), or expense (Sypro), and there were always limitations due to reproducibility issues with gels. 2D-DIGE dramatically improved with the synthesis of cyanine fluors a decade ago, which have a wide dynamic range and are very sensitive. While these dyes are expensive, they allow the unique ability to run three conditions on one gel, eliminating the reproducibility issues that existed between gels. Each of the three dyes has a different excitation and emission wavelength, which allows one gel to be scanned with a fluorescent scanner three times to get three perfectly overlapping images of samples labeled with different dyes. Spot volume ratios can be calculated with sophisticated software programs and the relative spot intensities can be compared to determine differentially expressed proteins. Spots with statistically different intensities can then be excised from the gel, in-gel digested, and their proteins can be identified via mass spectrometry. This technique has been applied to several systems and has helped reveal global changes within cells, allowing a broad view of the intricate changes that one stress can cause on its host.

Activity-Based Protein Profiling

Activity-based protein profiling (ABPP) is a relatively new method of measuring protein activity through the use of active-site, directed probes. Whereas traditional proteomics generally considers the presence or absence of a protein, activity-based protein profiling allows a direct measurement of active proteins, which can reveal great insight to the mechanisms of a system; it is also the only approach that monitors the real-time biologically important changes that may be occurring. This idea was first reported in 1999 by Lui et al. when they created a biotinylated-fluorophosphonate tag attached to a probe for serine hydrolases [40].

Activity-based probes consist of two parts: the reactive group (RG) and the reporter tag, which may be connected through a linker region. The reactive group is designed to covalently bind to a nucleophilic region of the active site of a protein, while the reporter tag can be either a fluorescent, radioactive, or biotin molecule used to detect the protein (Figure 1).

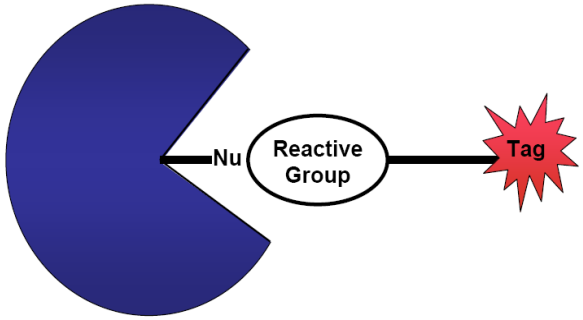

Figure 2. A schematic of an activity-based probe. Probes consist of a reactive group that is designed to covalently bind to a nucleophilic region (Nu) of the active site of an enzyme. The reactive group is linked to a detector tag, which is often a fluorescent, radioactive, or biotin group.

Activity-based probes have been designed for many families of enzymes and with different properties. Currently, probes exist for serine hydrolases [40,41], cysteine hydrolases [42,43], cysteine proteases [44-46], metalloproteases [47-49], tyrosine phosphatases [50-52], serine phosphatases [42], serine proteases [53,54], and many other families. The probes can be added to the sample as one molecule, or they can be added in two stages and assembled in a "click chemistry" manner. They have been used to label active enzymes in cell lysates, whole cells, tissues, and organisms. They have also been designed with different degrees of cell permeability and with varying binding constants. It is also common for similar reactive groups to be linked to multiple fluorescent tags for multiplexing analysis within a family of enzymes.

These probes are particularly useful in monitoring the change in activity of a group of proteins in the presence of a stressor over time. With fluorescent tags, the activity changes can be monitored through fluorescence imaging in cells, by fluorimetric quantitation, or through fluorescent scanning of one-dimension or two-dimension gels. With a biotinylated probe, enzymes can be selectively isolated with streptavidin and analyzed by mass spectrometry or other methods. The avenues for activity-based probes are just being explored, but they have already proven to yield important information that is leading to a more detailed understanding of the complexities of protein interactions within the cell.

Purpose

This study investigated the proteomic changes that occur in norovirus infected cells through the model system of MNV and murine macrophage cells. Through 2D-

DIGE and ABPP, this study aimed to report changes in protein expression and activity over the duration of the infection. Specifically, this study examined the response of caspases initiated by infection in the host cell and further investigated the role of apoptosis during cell death. 2D-DIGE was used to gain a general perspective on proteomic changes from infection and ABPP was used to monitor changes in protein activity within the cell in real time. Together, these methods yielded novel insights to the consequences of a norovirus infection and the complexities of the viral-host interaction.

CELL AND VIRUS CULTURE

RAW 264.7 Cells

Background

RAW 264.7 cells were first mentioned in 1977 by Ralph and Nakoinz [55]; however, they were not fully characterized until 1978 by Raschke et al. [56]. This macrophage cell line originated through cellular transformations of mouse cells induced by Abelson murine leukemia virus (AMuLV) in a BAB/14 mouse and was established from ascites. Although the cell line was developed in the 1970s, a PubMed search of reports referencing the line reveals it did not become popular until 2000. Recently, it was found that MNV can be cultured in murine macrophage cells [21], which proved to be a good model system for norovirus [1,20].

Cell Culture

RAW 264.7 cells are an adherent cell line cultured in Dulbecco's Modified Eagle's Medium (DMEM) supplemented with 10% fetal bovine serum (FBS). For the purpose of these experiments, as per the Hardy lab protocol for culturing RAW 264.7 cells, a high glucose (4.5 g/mL) DMEM was used as the base for the media. The media was supplemented with 10% premium-select FBS, 10 mM HEPES, 2 mM L-glutamine, and 1% Penicillin-streptomycin. Cells were grown in an incubator at 37°C with an atmosphere of 95% air and 5% CO_2.

Cell seed stocks are stored in liquid nitrogen, and fully thawed before seeding in fresh medium. The starting flask was prepared with a warmed (37°C) medium prior to thawing the cells for limited exposure time between the frozen state and the cultured state. Once the flask was prepared a seed stock was removed from the liquid nitrogen storage and immediately put in the 37° C water bath to thaw. The seed stock was held and circulated in the water bath until it was completely thawed. Once thawed, the cells were slowly dispensed into the prepared flask. Cells were labeled and placed in the incubator overnight. On the following day the medium was replaced to remove the excess freezing medium. On the second day, the cells were ready to passage.

The RAW 264.7 cell passage method was acquired from C. Wobus through Katie Daughenbaugh (August, 2005). Although these are adherent cells, trypsinization is not recommended for lifting; rather, cells were gently scraped in media with a cell scraper. Once cells were suspended in the medium, cells were broken up through vigorous pipetting. This was done by pressing the tip of the pipette tightly to the bottom of the flask and expelling the medium; this forced the cells through a high-pressure stream of medium, breaking them apart.

Cells were maintained at a relatively low cell density. RAW 264.7 cells can grow quickly and become activated if overpopulated. Being macrophages, these cells will begin to lift and consume dead cells if left to overpopulate; this will result in an unhealthy population. Cells found to be overgrown were discarded. To avoid overgrowth, cells were kept at a low density by passaging cells at 80% confluency before a thick monolayer accumulated (Figure 3). Cells were passaged multiple times a week and were diluted to between 1/3 and 1/6 when re-seeding. Cell growth remains consistent through passages in

the high teens to low twenties; however, the Alliance for Cellular Signaling (AfCS) has published a RAW 264.7 cell maintenance protocol, which states that cultures can be passaged for up to three months before re-seeding. However, there is some evidence that these cells remain stable through 60 passages (K. Green, personal conversation).

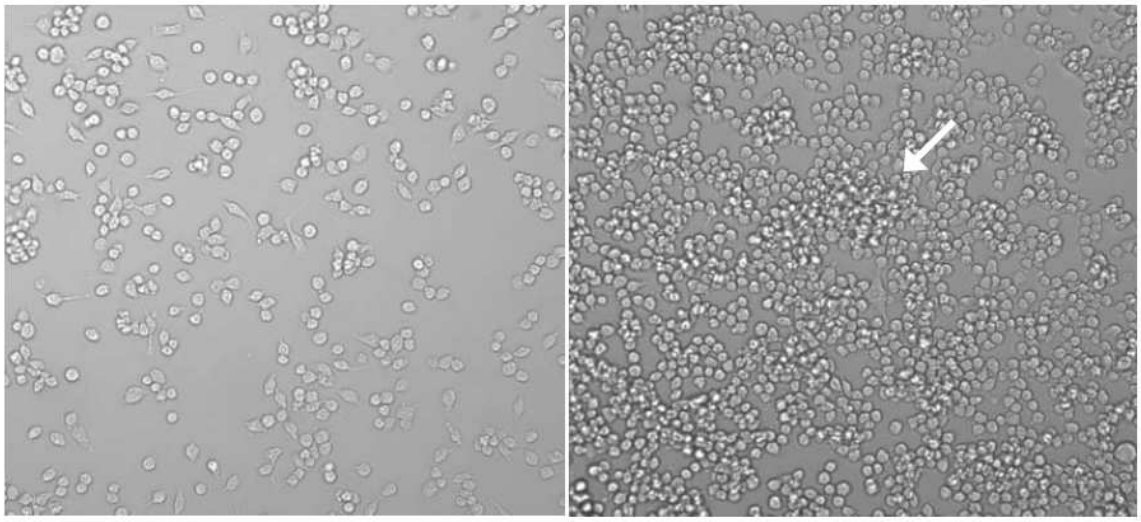

Figure 3. Low and high density cell growth images. RAW 264.7 cells should be maintained at low cell densities (left) and should be passaged at 80% confluency before thick monolayers form (right). Cell clumping is an indication of overgrowth (arrow).

Cell Freezing Procedure

The original stock of RAW 264.7 cells was acquired from the American Type Culture Collection. It was necessary to expand the cell stocks by creating subculture stocks by freezing low passage aliquots in liquid nitrogen. This allowed for multiple seeds from one source over several years to ensure reproducibility and to reduce costs.

Briefly, cells were scraped and centrifuged at low speed for ten minutes to pellet. The complete media was replaced with one milliliter of freezing media per 1 x 10^7 cells collected. While the ATCC recommends freezing subcultures of RAW 264.7 cells in complete medium with 5% DMSO (ATCC website), the Hardy lab recommends a

freezing media of 90% FBS and 10% DMSO (Kathy Jutila, personal conversation). Cells were gently mixed and one milliliter aliquots were pipetted into two milliliter cell freezing vials. Vials were labeled with the cell line, passage number, fraction of cells and type of container the cells were collected from, and initials. Vials were frozen slowly at -80°C in Styrofoam holders for 24 hours, after which they were moved to storage in liquid nitrogen. Cells were only harvested for subculture storage during their log-phase growth. Using unhealthy cells as seeds increases the odds of a failing flask during later experiments.

Cell Counting and Viability

Counting cells and determining cell viability is crucial to maintaining a healthy cell population and quantifying cells in culture. Typical cell subcultures should have greater than 90 percent cell viability; however, our RAW 264.7 cell cultures were generally 85 percent viable. Although approximate cell counts were calculated for RAW 264.7 cells at confluency in a variety of flasks and dishes by K. Daughenbaugh (Table 1), it is recommended that cells be counted when working with a new protocol.

Table 1. Approximate cell counts for various cell containers

Container Description	Approximate Number of Cells
12-well plate	2.00×10^6 cells per well
6-well plate	5.12×10^6 cells per well
60 mm dish	1.15×10^7 cells per dish
10 cm dish	3.15×10^7 cells per dish
15 cm dish	4.20×10^7 cells per dish
T75 flask	4.00×10^7 cells per flask
T162/T175 flask	8.70×10^7 cells per flask

Cells were counted with a hemacytometer (Figure 4), and viability was determined with Trypan Blue staining, which only permeates compromised cell

membranes. A hemacytometer is a glass slide with a grid pattern engraved, which allows for an accurate count of the cells in a designated area per volume.

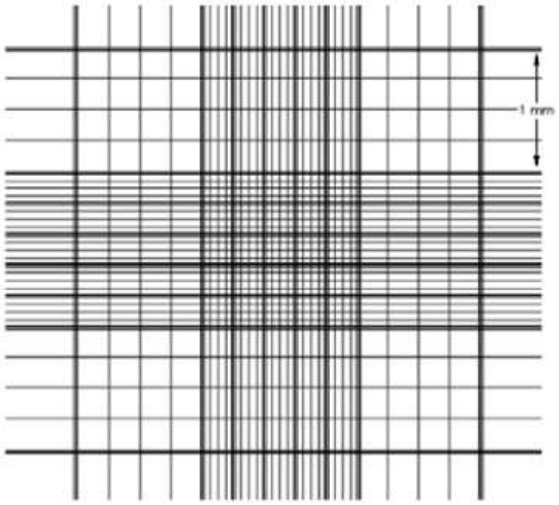

Figure 4. A diagram of a hemacytometer, a device used for counting cells and determining cell viability. This figure is from http://www.nalgenunc.co.jp/data/technote/3-25.htm.

Briefly, cells were dispensed onto the slide through a chamber inlet and viewed at 100x or greater magnification, whichever allowed for a full view of the grid. Cells were counted with a hand-held counter in each of the four perimeter squares and averaged. Each square should have between 20 and 50 cells; if the cell density is too high, the sample should be diluted. It is important to develop a consistent method for counting cells, such as only counting cells that touch the bottom and right box perimeters, not the top and left; this will ensure that each cell is only counted once. It is also important that cells be fully separated when counting, as clumps of cells can cause inaccurate counts. If cells are not sufficiently separated, mix by pressure pipetting until they are.

After the cell counts were averaged, the total cell per milliliter density and the percent cell viability were determined. The total cell count was determined with the following equation:

$$\text{cells/mL} = N \times D \times 10^4$$

where N is the average number of cells counted per square and D is the dilution factor. The value 10^4 was added to take into consideration the volume of the hemacytometer chamber. To determine the percent cell viability, cells were stained with Trypan Blue prior to loading on the hemacytometer; dead cells took up the dye, while healthy cells remained unstained. Both the total number of cells and the number of stained cells were counted. The percent viability was calculated as follows:

$$\% \text{ cell viability} = [(N_T - N_S)/N_T] \times 100$$

where N_T is the average total number of cells counted per square and N_S is the average number of stained cells per square.

Murine Norovirus

Virus Culture

As with the cells, the virus must be cultured to keep a working stock. Virus culture is similar to cell culture such that the virus is grown, expanded, and stocks are kept frozen. Unlike cell culture, virus stocks lose infectivity with each passage; therefore, it is necessary to calibrate the virus's infectivity with each passage by determining its titer. The virus titer refers to the number of plaque forming units per milliliter of virus, where a plaque is assumed to be formed by one infectious virus particle. While there may be millions of virus particles in the stock, only a small fraction of these particles will actually cause an infection. Each time a virus is passaged, the infectivity of the stock can change, so a plaque assay must be performed to determine its titer.

To expand virus stocks through natural replication, RAW 264.7 cells were seeded in large culture flasks (175 cm^3) at low cell densities (1:5 to 1:10) and incubated at 37° C overnight or until the flasks are at 50-75% confluency. Cells were at a low density to ensure they were in log-phase growth and healthy; this also ensured that cells would not die prematurely from overcrowding and reduce the efficiency of the virus replication. Cells were infected by replacing the DMEM with 10 mL of DMEM and concentrated virus at a low multiplicity of infection (MOI) (0.01 to 0.5). Cells were incubated at 37° C for exactly 48 hours until infection was terminated by placing the flasks at -80° C. Cells were lysed with three freeze-thaw cycles at -80° C and room temperature alternately. Flasks were scraped and all cells and media were collected and pooled. Cellular debris was pelleted via centrifugation at 1,500 x g for 15 minutes, centrifugation was repeated with the collected supernatant, and the pellets were discarded. The supernatant was collected, aliquoted, and stored at -80° C for later use. The virus titer was determined by plaque assay for each passage before the virus was used in later experiments.

Virus titer was determined in these experiments by plaque assay with crystal violet staining. The day prior to infection, RAW 264.7 cells were plated at a cell density of 2 x 10^6 cells per well in 6-well plates. Cells were incubated overnight at 37° C with 5% CO_2. Media were aspirated and cells were infected in duplicate with virus dilutions of 10^{-3} to 10^{-7} in DMEM to a total volume of 0.8 mL; 0.8 mL of DMEM alone was added to two wells as a control. Plates were gently rocked for one hour in the dark at room temperature. Media were aspirated and replaced with 2 mL of agarose overlay (1.5% SeaPlaque agarose, 1x Minimum Essential Media, 10% FBS). Overlay was prepared by adding pre-warmed agarose (50° C) to complete 2x MEM warmed to 37° C at a ratio of

1:1. The overlay was allowed to cool briefly to 40° C before adding it to the cells. Once added, the plates were left uncovered to cool and solidify under sterile conditions for 10 minutes. Plates were covered and given an additional 10 minutes at room temperature to ensure overlay solidification. Once completely cooled, plates were turned upside-down and returned to the incubator for 60 hours.

After the cells were allowed to incubate the cells were stained. Plates were removed from the incubator and fixed with 3.7% formaldehyde at room temperature for four to six hours. Overlay plugs were carefully removed with a pressurized stream of water aimed at the edge of the well. Excess water was tapped out of the wells, and the cells were stained with 0.5 mL 0.1% crystal violet in methanol:water v/v for 20 minutes gentle rocking at room temperature. The cells were briefly rinsed by inverting the plates into a pool of water and gently scooping the water into the wells. Plates were patted dry and plaques were counted and averaged in wells containing distinct plaques to determine the virus titer (Figure 5).

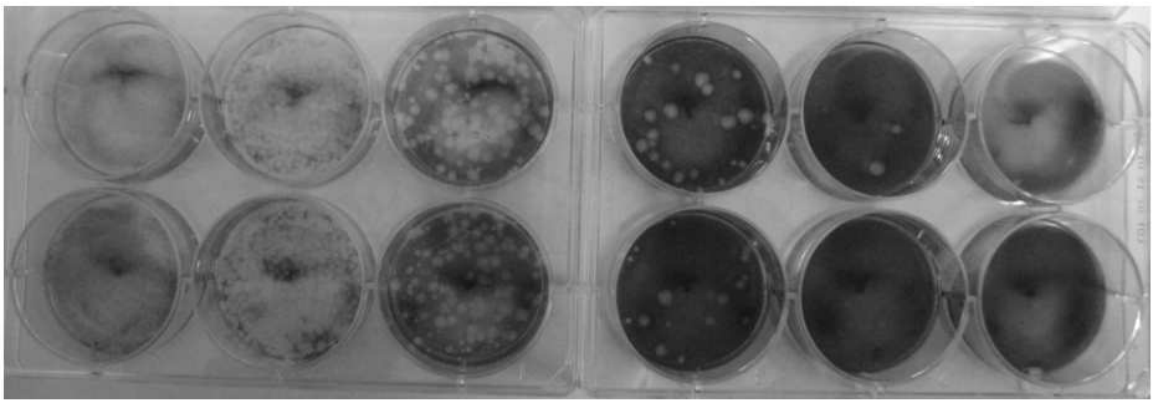

Figure 5. A plaque assay using crystal violet staining was used to determine the titer of a MNV stock. Wells contain virus dilutions ranging from 10^{-3} (left) to 10^{-7} (second from right) and a blank (right). Top and bottom wells are duplicate pairs. Plaques were counted in the 10^{-5} and 10^{-6} wells. Based on plaque counts, this virus culture was determined to have a titer of 2.4×10^{7} pfu/mL.

The equation for calculating the virus titer, or plaque forming units per milliliter (pfu/mL), is as follows:

$$\text{Virus Titer} = \frac{(P)x(1/D)}{V}$$

where, P is the number of plaques counted and averaged over at least two wells (this should be between 50 and 200 plaques); D is the dilution of virus added to the well where the plaques are counted; and V is the volume of virus media added to that well. For example, if 0.5 mL of a virus stock was plated at dilutions ranging from 10^{-3} to 10^{-7} in duplicate, and there were a countable number of plaques in the 10^{-6} dilution wells, then one would count the number of plaques in the duplicate wells, find their average, and this would be the value for P. The dilution value (D) in this example is 10^{-6}, and V is 0.5 mL; therefore, the pfu/mL for this example is P x 10^{6} pfu/0.5 mL.

Virus Purification

A common method of virus purification uses a cesium chloride (CsCl) gradient to separate virus particles of a known density. Virus particles in solution will migrate to the appropriate CsCl layer based on the density gradient formed by the CsCl after several hours of ultracentrifugation. A virus's density can be calculated based on the ratio of nucleic acids to proteins, where the buoyant densities of single-stranded RNA and proteins are 1.8 g/cm^3 and 1.3 g/cm^3, respectively. An appropriate CsCl density gradient can be made based on the calculated density of the virus particles, and the virus layer can then be collected. CsCl can be removed by dialysis against PBS for further purification.

Virus was purified according to the MNV-1 purification procedure provided by the Hardy Lab. RAW 264.7 cells were cultured in seven T175 flasks in 10 mL of DMEM

for 48 hours; six of the flasks were infected with MNV at an MOI of 0.01, while the seventh flask was used as a control. Cells underwent three freeze-thaw cycles at -20° C and room temperature before being harvested via scraping. Infected cell media was pooled and cellular debris was pelleted by centrifugation for 15 minutes at 3000 rpm. The supernatant was transferred to a clean tube and centrifugation was repeated to ensure all debris was removed. The supernatant was divided into two SW28 ultracentrifuge tubes and the volume was increased with sterile PBS. A 4 mL 30% (w/v) sterile sucrose cushion was dispensed underneath the media. The sample was centrifuged at 25,000 rpm for 3 hours at 4° C using rapid acceleration with an applied brake. The supernatant was discarded and the pellet was re-suspended in 5 mL total volume of sterile PBS supplimented with 1 mM $CaCl_2$ and 0.5 mM $MgCl_2$. The virus was overlaid on a 1.335 g/mL CsCl gradient in a SW55 ultracentrifuge tube and centrifuged at 35,000 rpm for 18 hours at 18° C with a slow acceleration and no brake. A large, diluted band was extracted from the gradient with a syringe and transferred to a Pierce 0.5 mL to 3.0 mL capacity dialysis cassette with a 10,000 molecular weight cutoff for dialysis. The sample was dialyzed against sterile PBS fortified with 1 mM $CaCl_2$ and 0.5 mM $MgCl_2$ overnight at 4° C with one PBS exchange, aliquoted, and stored at -80°C.

After several failed attempts at purifying the virus, virus purification was abandoned. Unfortunately, a discrete band never formed in the CsCl gradient after ultracentrifugation. On two occasions a very broad band was collected for dialysis, but upon completion of a plaque assay it was determined that the virus titer was too low (1 x 10^5 pfu/mL), and the method proved inefficient.

Due to the low titer resulting from purification, further analysis on the purified virus samples was conducted. Both purified and non-purified virus particles were analyzed with one-dimensional sodium dodecyl sulfate polyacrylamide gel electrophoresis (SDS-PAGE). Briefly, 50 µL each of two purified virus samples (p109 and p113) and one non-purified virus sample (p105) were mixed with 25 µL of 2x sample buffer with 40 mM dithiothreitol (DTT). Samples were boiled at 98° C for 5 minutes and briefly centrifuged at 13,000 rpm to collect condensation. The samples were loaded onto a 4-20% gradient SDS-PAGE gel (Pierce) in 1, 5, and 20 µL volumes (Figure 6). Lanes 6 and 7 are duplicates of p113 due to complications with loading the sample. Lane 1 contains 2 µL of Precision Plus Protein™ Dual Color Standard (Bio-Rad) protein standard.

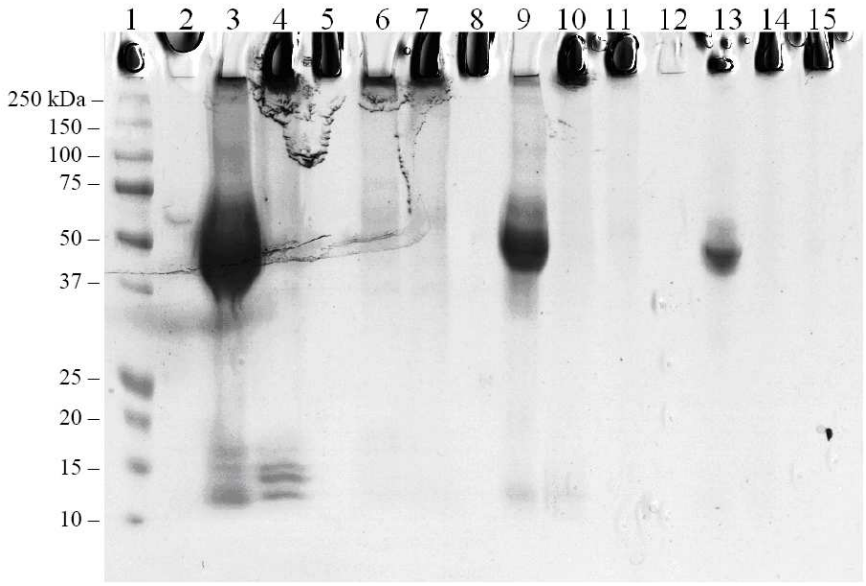

Figure 6. Purified virus particles. Multiple volumes of purified and non-purified virus cultures were analyzed on a 4-20% protein gel. Two purified virus cultures were unstable and fragmented (p109: lanes 4, 10, and 14; p113: lanes 6, 7, 11 and 15), while the non-purified virus culture (p105) remained intact (lanes 3, 9, and 13). Lanes 2, 5, 8 and 12 were left blank. Lane 1 is a protein standard.

The results from this gel reveal that intact virus capsid proteins are only present in the non-purified virus (p105) as is evident by the large band at ~50 kDa (lane 3). The p109 purified virus has some smaller protein bands (13-15 kDa), which may be fragmented capsid protein. The p113 purified virus only has a very faint band at 60 kDa, which is most likely from the intact virus capsid protein. Because the non-purified virus culture is in DMEM with FBS, it was necessary to analyze the media to eliminate the possibility that the protein bands from this gel were from media-related proteins.

Samples were prepared by adding 30 μL of 4x sample buffer containing 40 mM DTT to 30 μL of each of the aforementioned virus samples and an additional media sample consisting of fortified DMEM culture media. Samples were boiled at 98° C for 5 minutes and spun briefly at 13,000 rpm to collect condensation. Samples were each loaded in 10 and 20 μL volumes on a 4-20% SDS gel along with 2 μL of the protein standard (Figure 7).

Results from the gel electrophoresis indicate the large band at 60 kDa is not a product of the media. Only the non-purified virus sample p105 contains a large band at 60 kDa, suggesting that only this sample contains a large amount of virus protein. This gel also reveals that during virus purification the media-related proteins were not removed from the sample, as is evident by the similar banding patterns between the media alone (lanes 3 and 8) and the purified virus sample p113 (lanes 6 and 10). The presence of multiple protein bands in the purified virus sample p109 also indicates that several proteins are purified during the virus purification process, and the presence of the virus protein in p109 is undetectable.

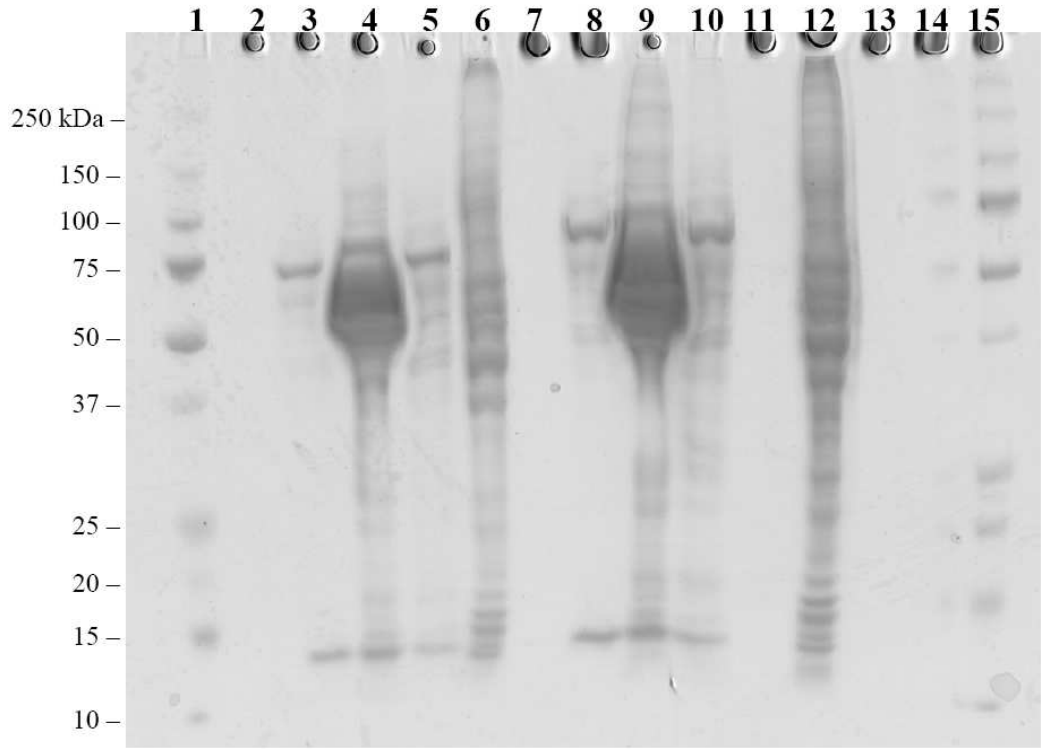

Figure 7. Analysis of purified and cultured virus particles and media-related proteins at 10 and 20 μL volumes. Only the non-purified virus sample p105 has a large virus capsid protein band at ~60 kDa (lanes 4 and 9). Purified virus sample p109 appears to have several different sized proteins (lanes 6 and 12), while purified virus sample p113 (lanes 5 and 10) has a banding pattern similar to the media alone (lanes 3 and 8). Lanes 2, 7, 11, 13, and 14 were left blank. Lanes 1 and 15 contain a protein standard.

The results from these two gels explain why the virus titer from the purified virus samples was so low. Without intact virus capsid protein, the purified virus samples seem to have little to no viable virus particles in them. These results suggest that the capsid protein is not surviving the purification processes, and perhaps the capsid is being cleaved into smaller fragments, which would explain the low molecular weight (~15 kDa) protein bands in both gels.

Infecting Cells

Multiplicity of Infection

When infecting cells, it was important to have a ratio of greater than one virus particle per cell to ensure the majority of the cells were infected. Cells have been infected with MNV at a multiplicity of infection (MOI) of 0.05 [24] and higher . The MOI is the ratio of virus particles per cell. To determine the volume of virus to add to cells, the following formula was used:

$$V = (MOI \times N)/T$$

where V is the volume in milliliters of virus, N is the number of cells being infected, and T is the pre-determined virus titer in pfu per mL.

Monitoring Cell Growth and Viability during Infection

Cell growth and viability were monitored during the initial 24 hours of infection with MNV. Prior monitoring of the cells by the Hardy lab indicated that the majority of cells infected with the virus are dead 24 h.p.i. (personal conversation).

Briefly, 2×10^6 cells were plated per well in 6-well plates and left to adhere overnight at 37° C. Cell media was replaced with fresh media (control samples) or new media plus virus at an MOI of three. Cells were returned to the incubator and collected in triplicate and counted at 6, 12, 18, and 24 h.p.i. per the aforementioned cell counting method. Cell percent viability was calculated using Trypan Blue. The percent infected-cell viability was normalized to the percent non-infected cell viability.

Cell growth was noticeably inhibited by the virus at 12 h.p.i.; while the total cell number continued to increase, it was marginal compared to the non-infected cell growth rate (Figure 8). Cell viability declined by the first time point and continued to decline to less than 20 percent viability by 24 h.p.i. These results are consistent with previous, non-documented observations made by the Hardy lab.

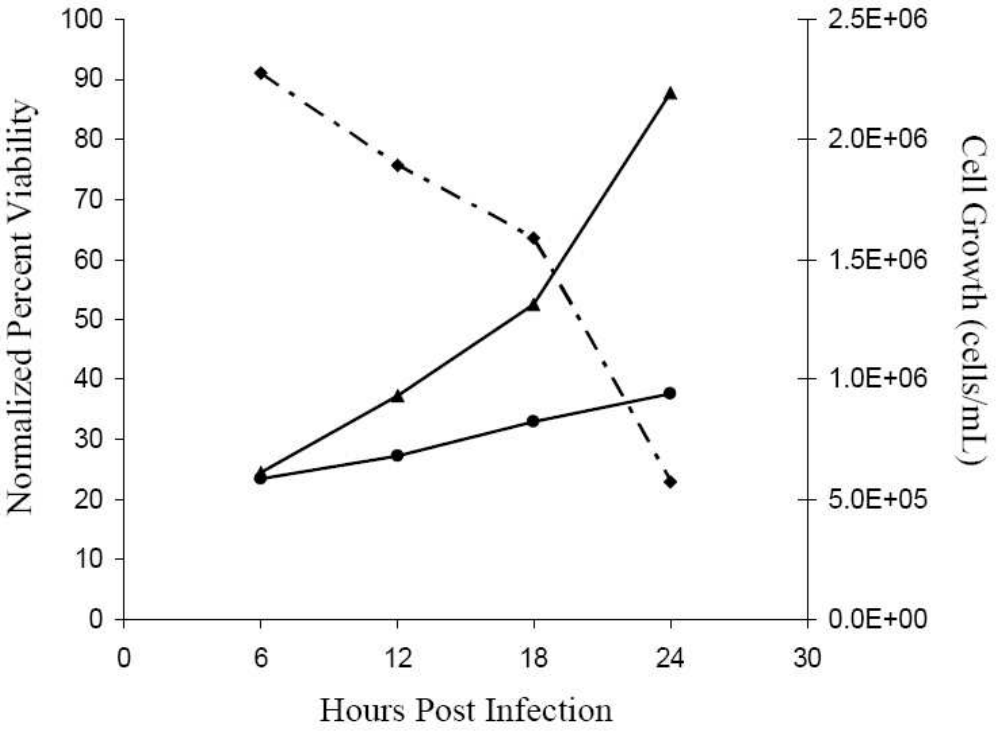

Figure 8. Cell counts of infected (●) and non-infected cells (▲) (right axis) and the percentage of viable infected cells to viable non-infected cells (left axis; dashed line) were recorded at 6, 12, 18, and 24 hours post infection. Viability was determined using Trypan Blue. *n*=3.

The viral progression is also visually apparent in the cellular morphology (Figure 9, Appendix A). Briefly, infected and non-infected cells were imaged 12 h.p.i. in the 6-well plate using an inverted microscope with 200x and 400x magnification. Non-infected cells appear plump and refractive, while infected cells have elongated appendages and have more apparent internal membranes. By 18 h.p.i. a majority of infected cells will

begin to lift from the plate, which is also a sign that the infection has progressed. These changes in cell morphology and adherence have been consistently observed throughout many infections.

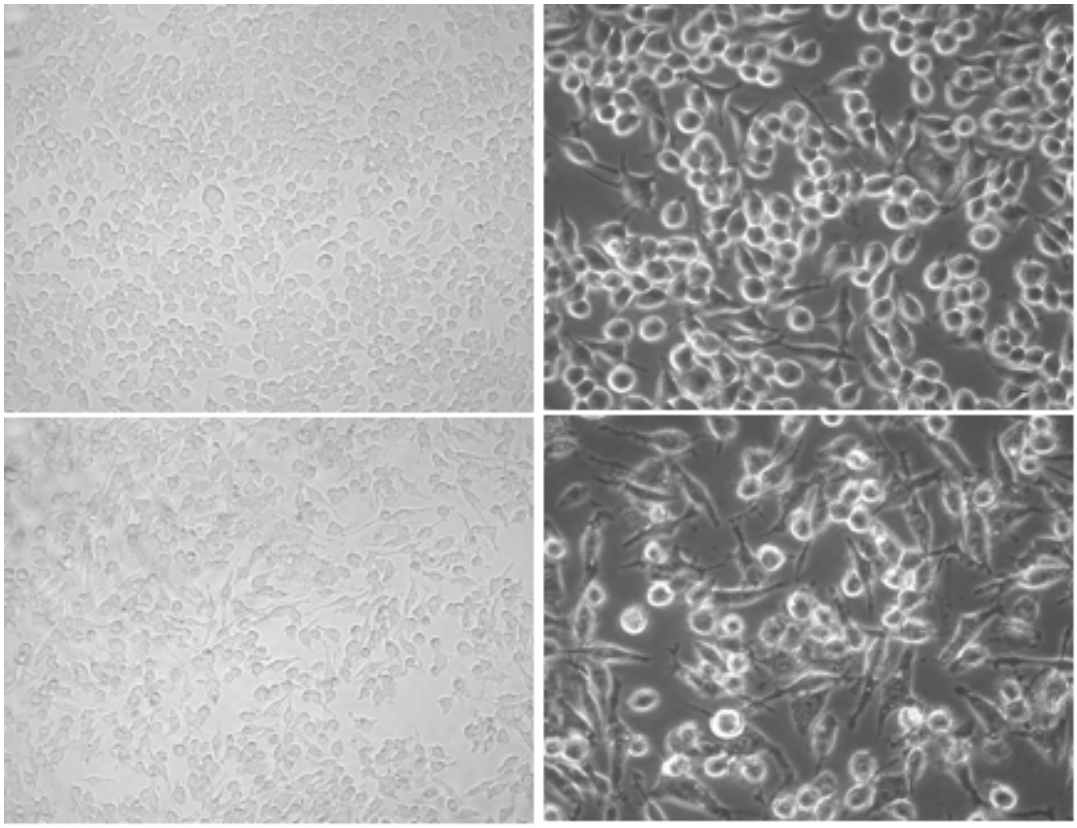

Figure 9. Healthy cells versus infected cells. Infected cells (bottom) appear to have more appendages and membrane rearrangement. Healthy cells (top) appear spherical or lemon-shaped and plump. Left images are at 20x magnification and right images are at 40x magnification.

VIRALLY INDUCED PROTEOMIC CHANGES

Background

One technique for monitoring global proteomic changes in cells is two-dimensional differential gel electrophoresis (2D-DIGE). In the last decade, with the development of protein-labeling fluorescent dyes and the advancement of sophisticated software programs, 2D-DIGE has become a powerful tool for understanding proteomic changes in stressed cells. Common stressors include drugs[57-59], oxidative stress[60], and viral infection[61-63].

This chapter examines the results of a 2D-DIGE experiment comparing infected and non-infected cells at 4 and 12 h.p.i. While this experiment is a brief look at the proteomic changes that occur during a norovirus infection, the results were surprisingly consistent with changes that occur during apoptosis.

Experimentation

Cells were grown in DMEM, infected with an MOI of 0.1, and collected at 4 and 12 h.p.i. Cell suspension was aliquoted and pelleted. Pellets were combined to make working pellets of 3.0×10^7 cells per pellet.

Cells pellets underwent three freeze-thaw cycles of 15 minutes per environment at -80ºC and room temperature. Cell pellets were solublized in 100 μL Chaps/Urea buffer with 40 mM DTT and 5 μL DNase-RNase by gentle pipetting followed by tumbling at room temperature for 1 hour. Samples were spun at 15,000 rpm for 10 minutes at 18 ºC

to collect insoluble proteins. The supernatant was transferred to a new tube and five volumes of ice-cold acetone were added. Samples were left at -80ºC overnight to precipitate the protein. Samples were spun at 15,000 rpm for 10 minutes at 18 ºC to collect the protein pellet. The acetone was removed and the pellets were placed in a hood for 15 minutes to air dry.

Protein pellets were re-suspended in 100 uL Chaps/Urea buffer by tumbling at room temperature for 1 hour. Protein measurements were determined by a Bradford Assay, and protein concentrations averaged 6.9 μg/μL. 2 uL of DNase-RNase, 40 mM DTT, and 0.5% 3-11 NL ampholites were added to 500 μg of protein from each sample. Chaps/Urea buffer was added to a total volume of 480 μL. Samples were centrifuged at 15,000 rpm for 10 minutes at 18 ºC to pellet any insoluble proteins remaining.

Samples were focused on a 3-11 non-linear, 24 cm IEF gel strip with an IPGphor until the focusing reached 45,000 total Volt-hours. IEF strips were reduced with 10 mg/mL DTT in an equilibration buffer followed by modification with 25 mg/mL iodoacetamide (IAA). Strips were loaded onto 12.5% polyacrylamide gels and covered with 0.5% agarose. Gels were loaded into an Ettan Dalt II System and run at 150 constant volts for 15 hours. Gels were rinsed briefly in dH_2O before being fixed in 50:10 methanol:acetic acid. A SyproRuby stain was applied overnight, and the gels were de-stained in 10:7 methanol:acetic acid for one hour, followed by de-staining in dH_2O for an additional hour.

Gels were imaged on the Typhoon scanner with 100 μm resolution at an excitation of 532 nm and an emission filter at 610 nm. After imaging, gels were stained

overnight with GelCode Blue staining reagent. Gels were de-stained with MilliQ water overnight with multiple rinses. Gels were re-scanned with an Epson 4180 Photo scanner.

SyproRuby-stained images from the Typhoon were quantitatively analyzed using the Progenesis SameSpots software. Gel images were aligned and normalized volumes were compared for differential expression levels. Spots having greater than a 2-fold increase or decrease were deemed "differential" and were selected for further analysis and identification. Of these differentially expressed proteins, there were 36 spots identified at 4 h.p.i. and 30 at 12 h.p.i., five of which were overlapping proteins. Spots were located and excised from the coomassie-stained gel and in-gel digested with trypsin. Using electrospray-ionization mass spectrometry and the MASCOT search engine, 44 spots were identified as 38 unique proteins (Figure 10, Table 2, Table 3).

Protein Significance

Of the 44 positively identified proteins, 30 of these have been correlated with apoptosis. Only 14 proteins have not been correlated to apoptosis in the literature, four of which are "unnamed" proteins. Some of these proteins affect apoptosis through the mitochondria, others are related to structural changes, and some are affected by caspases.

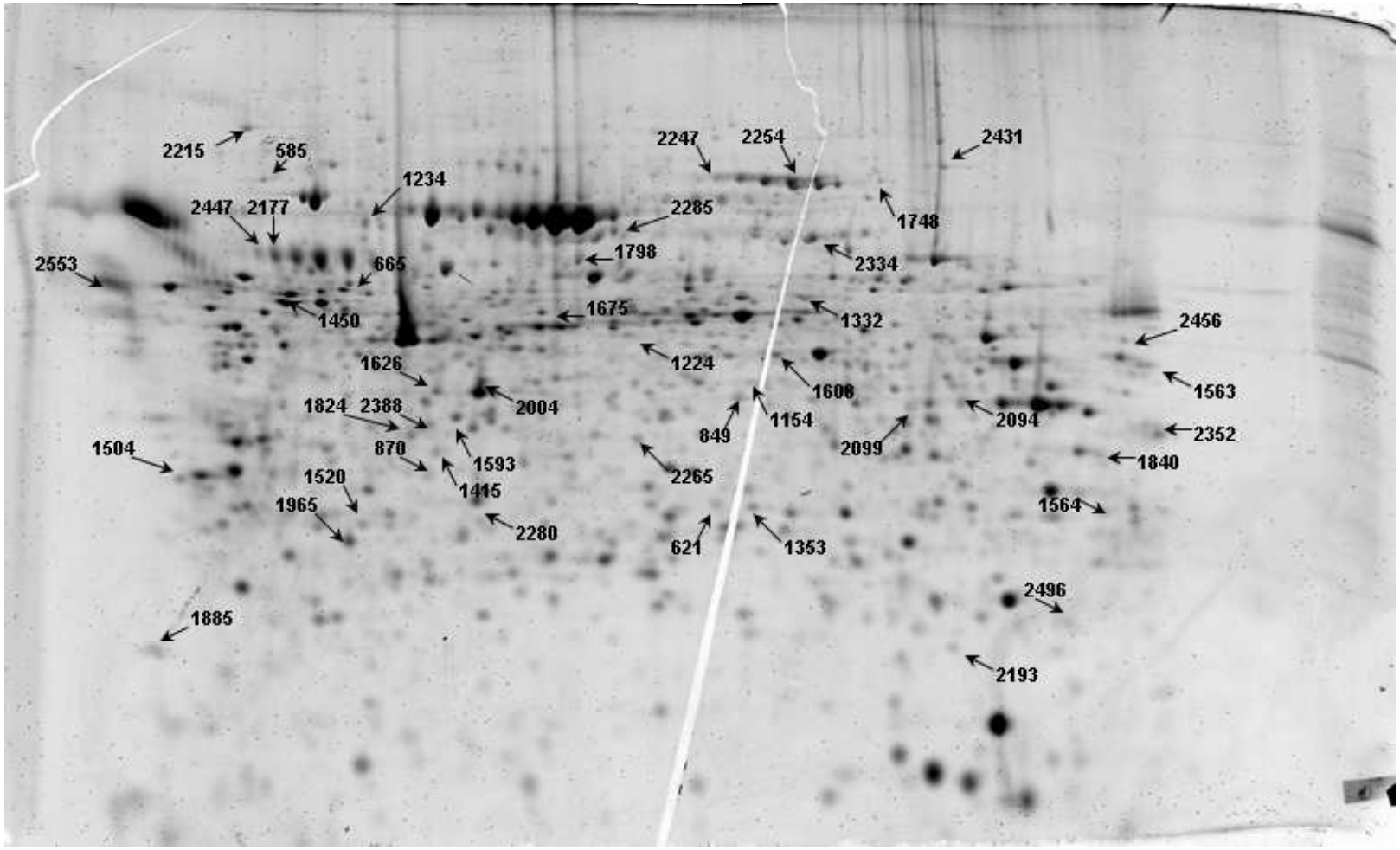

Figure 10. 2D-DIGE revealed 44 differentially regulated proteins at 4 and 12 h.p.i. The majority of these proteins can be linked to apoptosis.

Table 2. Differentially regulated proteins at 4 h.p.i.

Spot No.	Fold Change	Protein I.D.	Apoptosis Related	References
585	-9.6	heat shock 70kDa	Yes	64,65
1564	-3.7	ribonucleoprotein A3	Yes	66-68
1563	-2.7	ribonucleoprotein A3	Yes	66-68
2177	-2.5	gp96	Yes	69-71
1840	-2.5	voltage dependant ion channel 1	Yes	68,72-78
2285	-2.3	unnamed protein	Unknown	
2456	-2.2	glutamate oxaloacetate transaminase 2	Yes	79-81
1234	-2.1	lymphocyte cytosolic protein	Yes	82
2553	-2.0	calreticulin precursor	Yes	83
870	-2.0	annexin A4	Yes	84
1798	2.0	t-complex-type molecular chaperone	Unknown	
2496	2.1	tansgelin-2	Unknown	
1224	2.2	unnamed protein	Unknown	
2388	2.2	class I beta tubulin	Yes	85,86
2352	2.3	topoisomerase-inhibitor suppressed protein	Yes	87,88
2099	2.4	heterogeneous nuclear ribosome protein	Yes	88-92
2193	2.4	alpha enolase	Yes	93
2094	2.6	glyceraldehyde 3-phosphate dehydrogenase	Yes	94,95
2004	2.8	Beta-actin	Yes	86
1965	2.9	RhoGDP dissociation inhibitor	Yes	96,97
1885	3.0	telomerase binding protein	Unknown	
1748	3.3	aconitase 2	Unknown	
1674	3.5	ARP3 actin	Unknown	
1626	3.6	RIKEN cDNA	Unknown	
1593	3.7	alpha-3 chain tubulin	Yes	67,98
1520	3.9	RAN binding protein	Yes	99
1415	4.2	annexin A4	Yes	84

Table 3. Differentially regulated proteins at 12 h.p.i.

Spot No.	Fold Change	Protein I.D.	Apoptosis Related	References
621	-6.3	hydroxypyruvate isomerase	Unknown	
849	-5.9	nucleolin	Yes	100,101
1234	-4.9	lymphocyte cytosolic protein	Yes	82
1353	-4.4	phosphoglycerate mutase type B	Yes	102
1154	-3.2	DNA-type molecular chaperone hst70	Yes	103,104
1332	-3.0	aldehyde dehydrogenase AAHD-MI	Yes	105,106
2215	-2.5	gp96	Yes	69-71
1608	-2.4	ribonucleoprotein A1B	Yes	66-68
2254	-2.4	hemiferrin transferrin-like protein	Unknown	
2247	-2.3	transferrin-like protein	Unknown	
2280	-2.3	unnamed protein	Unknown	
2265	-2.2	chaperonin subunit 5	Unknown	
2334	-2.2	lamin C2	Yes	107
1504	-2.2	prepro protein	Unknown	
2431	-2.2	pyruvate kinase	Yes	84,108
1824	-2.1	spermidine synthase	Yes	109
1965	-2.0	RhoGDP dissociation inhibitor	Yes	96,97,110
1450	-2.0	vimentin	Yes	111-116
2447	2.2	gp96	Yes	69-71
1224	2.4	Unnamed protein	Unknown	
2094	2.6	glyceraldehyde 3-phosphate dehydrogenase	Yes	94,95
665	4.2	vimentin	Yes	111-116

The mitochondria play an important role in apoptosis, releasing cytochrome c into the cytoplasm and activating caspase-9, an initiator caspase responsible for activating effector caspases such as caspase-3. Cytochrome c is released into the cytoplasm after calcium accumulates in the mitochondria or when pores develop in the mitochondrial membrane from bcl-2 activation (Figure 11). Voltage-dependent ion channel (Vdac) has been shown to interact with bcl-2 [73]. It has also been shown that glyceraldehyde 3-phosphate dehydrogenase (GAPDH) is over-expressed in apoptotic cells, entering the mitochondria and interacting with Vdac and increasing the release of cytochrome c[77]. It is interesting to note that in this study GAPDH is up-regulated as in other studies; however,

Vdac is down-regulated, which seems to be contrary to what would be expected if it is important in developing the mitochondrial pores. A recent study suggests that Vdac is unnecessary for mitochondrial-mediated apoptosis[74]; however, in this study it clearly changes in abundance. Cytochrome c can also be released from the mitochondria after an accumulation of Ca^{2+}. One suggested role of annexin IV is as an ion channel responsible for regulating Ca^{2+} in the mitochondria. At 4 h.p.i., annexin IV is up- and down-regulated in two spots (Figure 12), which is indicative of a post-translational modification; however, no definitive post-translational modifications are currently known for annexin IV.

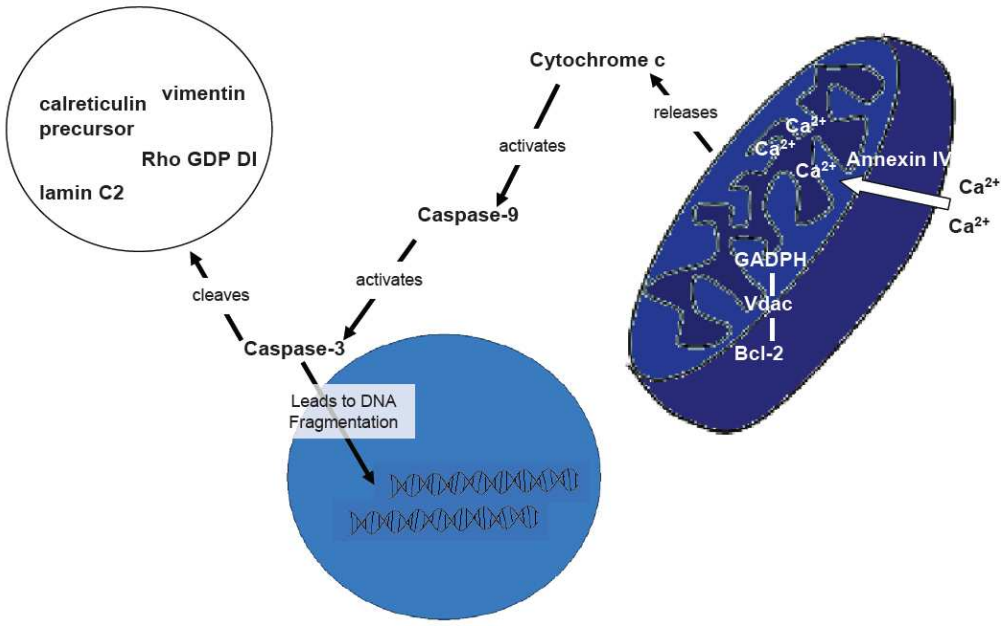

Figure 11. Schematic of differentially regulated proteins' interactions during apoptosis. An influx of calcium to the mitochondria through annexin IV and pores, which are created through interactions with Bcl-2, Vdac, and GAPDH, leads to the release of cytochrome c. Caspase-9, an initiator caspase activated by cytochrome c in the cytoplasm, activates caspase-3. Capsase-3 has several substrates, some of which are structural (vimentin), while others are regulatory (Rho GDP and calreticulin precursor).

Heat-shock protein 70 (hsp70) is also known to affect apoptosis at the mitochondrial level by interacting with Bax, a member of the Bcl-2 family, and preventing its translocation into the mitochondria[117], thereby blocking the release of cytochrome c from the mitochondria and preventing the activation of caspase-9[65]. Hsp70 is drastically decreased (9.4 fold) at 4 h.p.i., suggesting it is down-regulated to assist apoptosis.

Actin and tubulin, two major cytoskeletal proteins, are also affected by viral infection. These proteins increase during apoptosis, which correlates with previous findings that suggest that these proteins aid in the formation of apoptotic bodies[118]. Membrane re-organization is also well documented during apoptosis, which could be directly related to the increase in these proteins. Vimentin is also a filamentous cytoskeletal protein that is related to the flexibility of the cell's structure and has been shown to be cleaved by caspase-3[112,116]. Vimentin, like annexin IV, is also both up and down-regulated. At 12 h.p.i. vimentin is up-regulated 4.2-fold and down-regulated 2.0-fold in infected cells (Figure 12). Vimentin is known to undergo post-translational modifications; it can be phosphorylated[119] or s-nitrosated[120].

Several other proteins regulated during the infection are also characterized as caspase substrates. Rho GDP dissociation inhibitor is a substrate of caspases-3[96,97] and calreticulin precursor is a variant of Rho GDP dissociation inhibitor. At 12 h.p.i. Rho GDP dissociation inhibitor decreases 2.0-fold, which coincides with an increase in caspsase-3 activity (see Chapter 4). Lamin C2, a protein lining the inner nuclear membrane, is also cleaved by caspases [107].

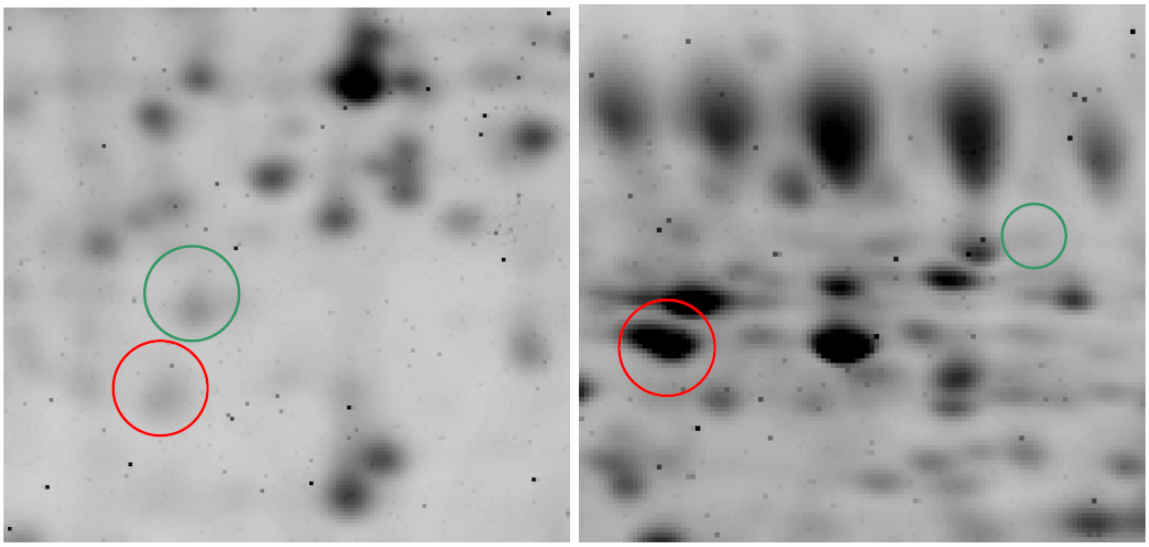

Figure 12. Proteins with potential post-translational modifications. Annexin IV is both up (green circle) and down-regulated at 4 h.p.i. Spot 1415 is up 4.2-fold during infection (green circle), while spot 870 is down 2.0-fold (red circle). Vimentin is up-regulated 4.2-fold at spot 665 (green circle) and down-regulated 2.0-fold at spot 1450 (red spot) in infected cells. These shifts may be indicative of post-translational modifications, increasing molecular weight and shifting the pI.

There is also a correlation between aconitase and transferrin, which are both regulated during infection. Aconitase-2 is a mitochondrial protein responsible for iron regulation and is also reciprocally correlated with superoxide levels[121]. At 4 h.p.i. there is a 3.3-fold increase in aconitase-2, which is suggestive of an increase in free iron. Transferrins are responsible for transporting iron, and at 12 h.p.i. there are two down-regulated transferrin-like proteins. This suggests that the cell may be inundated with iron and is trying to block incoming iron and sequester the free cellular iron. Iron homeostasis is important in controlling reactive oxygen species (ROS) activation, which, when activated, reduces aconitase-2 activity[122].

While its role in apoptosis is not fully understood, superoxide, an ROS, is a critical component of cell death. STAT1 signaling, which is regulated by caspase-3, is known to increase ROS during apoptosis[123]. In the presence of a caspase inhibitor,

superoxide levels increase and cells die[124]. STAT1-deficeint macrophage cells are unable to synthesize superoxide, which renders them unresponsive to caspase inhibition and allows them to survive[123]. STAT1 is also responsible for controlling ROS and iNOS[125], which induce apoptosis through s-nitrosation modifications[126]. Caspases, GAPDH, and vimentin, which are all regulated during MNV infection, undergo s-nitrosation[120]. Decreased superoxide levels were also recently correlated with apoptosis induced by sindbis virus[121]. The mechanisms of ROS in apoptosis are not fully characterized; however, these data suggest ROS may be involved in MNV-mediated apoptosis.

INVESTIGATING CASPASE ACTIVITY

Background

Caspases play a vital role in apoptosis, and inhibiting their activity can prevent it from occurring. The correlation between caspase-3 (or, interleukin-1 beta converting enzyme, ICE) and apoptosis was first described in 1994 [127] when over-expression of ICE increased cell death and point mutations in this protein prevented cell death. A PubMed search for "caspase AND apoptosis" reveals over 27,000 papers published since the early 1990s. These results alone suggest the importance of caspase activity and its role in apoptosis.

While apoptosis has been correlated and well characterized with several viruses, such as HIV [128], adenovirus [129], hepatitis C virus [130], herpes simplex virus [131], human papillomavirus [132], and influenza virus [133], the correlation between infection and cell death has not been thoroughly investigated for caliciviruses. Only FCV has been shown to induce apoptosis via an increase in caspase activity [33,38,134,135].

Caspase activity can be monitored in cells with a variety of activity-based probes. Immunochemistry Technologies, LLC manufactures apoptosis detection kits with probes targeting active caspases. These probes are either a carboxyfluorescein (FAM) or sulforhodamine (SR) FLICA; FLICA stands for fluorochrome inhibitor of caspases. FLICA kits exist for specific caspases and as pan-caspase detectors. These probes are membrane permeable and covalently bind to the active sites of the selected caspases via a small peptide (~4 amino acids) with an aspartic acid residue. Once the probes are bound,

cells can be analyzed for caspase activity qualitatively with fluorescent microscopy or quantitatively through flow cytometry or with a fluormetric plate reader.

Visualizing Caspase Activity

Caspase activity was qualitatively monitored in infected and non-infected cells during the first 12 hours of infection. The pan-caspase probe, SR-VAD-fmk, was used to detect the overall caspase activity, while caspase-2 and caspase-3/7 were detected with the FAM-VDVAD-fmk and FAM-DEVD-fmk probes, respectively.

Cells were initially probed with SR-VAD-fmk to detect the total caspase activity during infection. Cell labeling was done according to the FLICA manual with slight modifications. Cells were seeded in 1.0 mL of DMEM at a density of 1 x 10^6 cells per well in 12-well plates and allowed to incubate at 37° C one day prior to infection. Cell media was aspirated and replaced with 1.0 mL fresh DMEM or DMEM plus virus at an MOI of 5. Every two hours from 0 to 12 h.p.i. one infected and one non-infected well were labeled with the FLICA, while one infected and one non-infected well were left un-labeled. The 0 time point was 5 minutes of virus exposure prior to labeling. For each time point the media was aspirated and replaced with either 500 μL of DMEM containing 1x FLICA (labeled) or 500 μL of DMEM (un-labeled). Cells were allowed to incubate in the dark at 37° C for one hour; twice, the plates were gently tilted to distribute the probe. Cells were washed three times with 1.0 mL DMEM for 5 minutes and 500 μL of fresh DMEM were added to the cells before imaging.

Cells were imaged directly in the plate wells using an inverted fluorescent microscope (Nikon TE300). Digital images of each sample at 400x magnification were taken using OneSpot software.

Results show an increase in total caspase activity as early as 2 h.p.i. in infected cells compared with non-infected cells (Figure 14). Non-infected cells remain mostly un-labeled throughout the 12 hours, while infected cells seem consistently labeled from 2 to 10 h.p.i. At 12 h.p.i. infected cells begin to lift from the culture plate and stain an intense red (Figure 13). The labeled cells in the control samples can be explained due to naturally occurring apoptotic cells, which can represent 2-6% of the cell population (Immunochemistry Technologies, LLC).

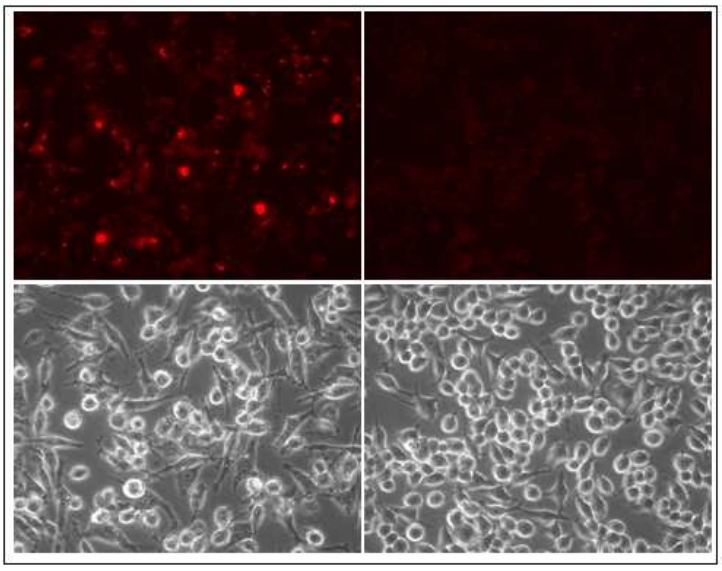

Figure 13. Fluorescent and non-contrast images of infected (left) and non-infected (right) RAW 264.7 cells stained with the pan-caspase activity-based probe, FLICA, at 12 hours post infection. Non-infected cells appear plumb and unstained, while infected cells appear elongated with possible intra-membrane reorganization and additional appendages. Cells become stained an intense red and begin lifting from the culture plate at 12 hours.

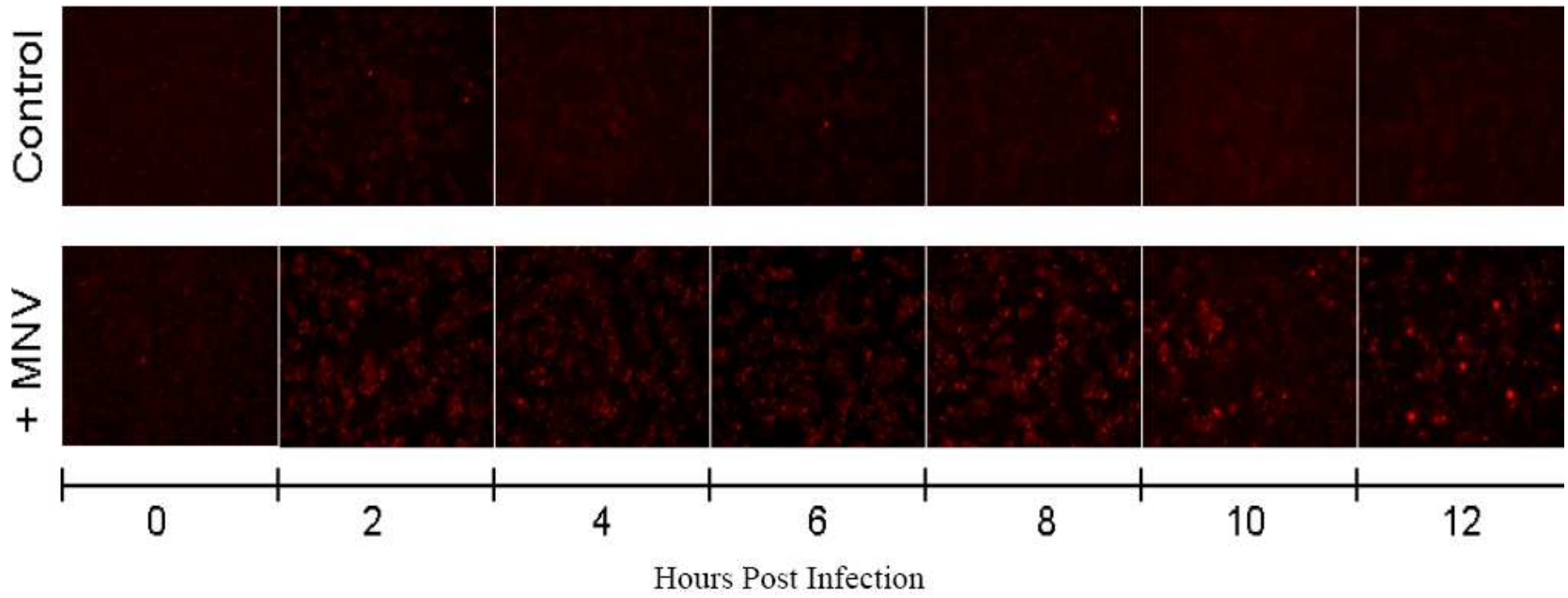

Figure 14. Images of infected (bottom) and non-infected (top) RAW 264.7 cells stained with the pan-caspase activity-based probe, FLICA, during the first 12 hours post infection. Non-infected cells remain unstained, while infected cells become stained by 2 h.p.i.. Images were taken with a Nikon TE300 inverted microscope at 400x magnification.

Cells were also labeled for caspase-2 and caspase-3/7 activity. Due to the inherent similarities between the active sites of capase-3 and caspase-7 there is only one probe, thus their activities cannot be individually monitored.

Cells were prepared as described above prior to infection. Cells were infected at an MOI of 4 and allowed to incubate in the dark at 37° C for 1.5 hours. All media was then aspirated and replaced with 0.5 mL of fresh DMEM and cells were returned to the incubator. At 12 h.p.i. the media was aspirated and cells were labeled with 0.5 mL of 1x SR-VAD-fmk, FAM-VDVAD-fmk, FAM-DEVD-fmk, or a combination of SR-VAD-fmk and one of the FAM probes in DMEM. Samples were allowed to incubate at 37° C for 1 hour. Media was again aspirated and 1.0 mL of 1x wash buffer from the FLICA kit was added to each well for 5 minutes and washing was repeated once. Wash buffer was replaced with 300 μL of wash buffer before imaging.

Although cell images were taken, insufficient data were collected to determine changes in caspase-2 and caspase-3/7 activity levels due to infection. However, one image should be noted, as it clearly shows co-localization of caspase-2 FLICA with the pan-caspase FLICA (Figure 15). The cells in this image show areas of co-localization of the two probes; however, of more interest are the areas labeled with only the pan-caspase FLICA, which indicate activation of other caspases. It is also interesting to note when comparing the non-contrast image to the multiplexed fluorescent image there is one un-labeled cell, which does not have any active caspases. Images co-stained with the pan-caspase FLICA and caspase-3/7 FLICA yielded similar results.

Results from these two qualitative analyses indicate a virally-induced increase in caspase activity by 2 h.p.i. The pan-caspase activity signal intensifies at 12 h.p.i. when

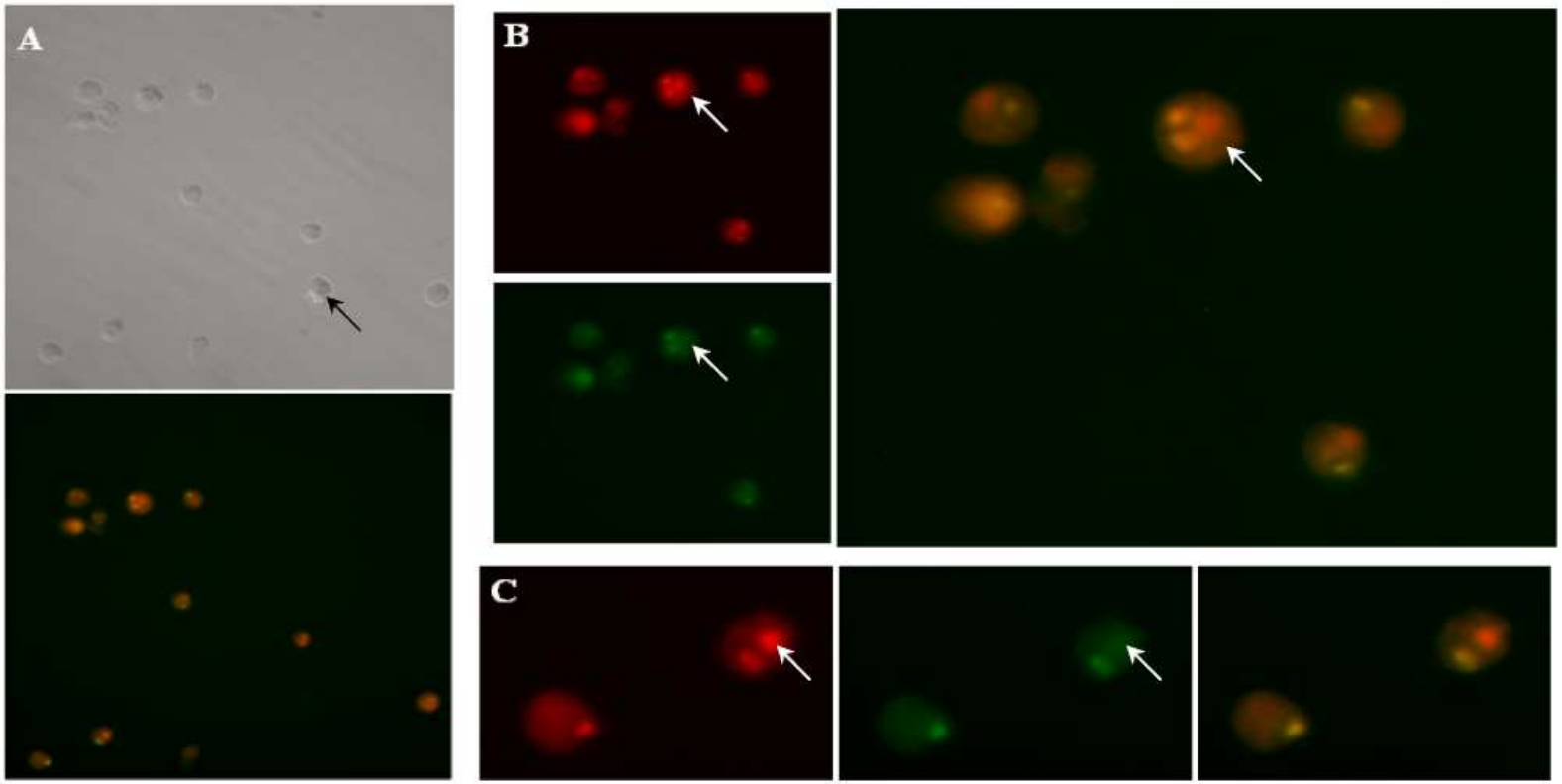

Figure 15. Multiplex imaging of caspase activity in MNV-infected cells. Cells were labeled with a pan-caspase FLICA, SR-VAD-fmk, and a caspase-2 FLICA, FAM-VDVAD-fmk. All active caspases are stained red, while only active caspase-2 proteins are stained green. Caspase activity was present in all but one cell in this frame (arrow in A). A diffuse staining of both probes was present in the cells (B and C). Localized areas of concentrated caspases can be seen in each cell with varying amounts of each probe, indicating that the pan-caspase FLICA is labeling more than caspase-2.

cells begin to lift from the culture plate. The multiplexing analysis revealed positive labeling for caspase-2 and caspase-3/7 activity at 12 h.p.i. in infected cells (images not shown). Cells showed some co-localization of the pan-caspase FLICA with both the caspase-2 and caspase-3/7 FLICAs, but co-localization did not account for all of the pan-caspase activity. Incomplete co-localization should be expected and can be explained by the activity of several other caspases, which were not specifically targeted, such as caspases 1, 4, 8 and 9.

Comparing Caspase Activity through Gel Electrophoresis

After cells were visualized by fluorescent microscopy they were scraped and harvested for further analysis via gel electrophoresis. Cells were centrifuged at 13,000 rpm for 10 minutes and the supernatant was discarded and replaced with 40 μL 4x sample buffer containing 40 mM DTT. Samples were boiled for 5 minutes, centrifuged to collect condensation, re-boiled, and centrifuged at 13,000 rpm for 10 minutes. A total of 20 μL of each sample was loaded onto a 4-20% SDS gel and run at 200 Volts for 45 minutes. The gel was immediately rinsed in dH_2O and imaged on a fluorescent scanner with a 532/610 filter set at 900 PMTs (Figure 16).

The results from the 1D gel show several intensified protein bands in the infected cells beginning at 2 h.p.i., which is consistent with the qualitative data. The 8 h.p.i. samples are non-FLICA labeled cell proteins that were accidentally switched with the FLICA-labeled samples. These lanes surprisingly yield a fluorescent band, which could be the result of an auto-fluorescent protein. At 12 h.p.i. a low molecular weight protein is present in the infected samples, which was not present at earlier time points.

Unfortunately, attempts to excise and identify the protein bands using in-gel digestion and electrospray-ionization mass spectrometry techniques were unsuccessful. Regardless of the protein's identification, 12 hours post infection is clearly an important time point during norovirus infection.

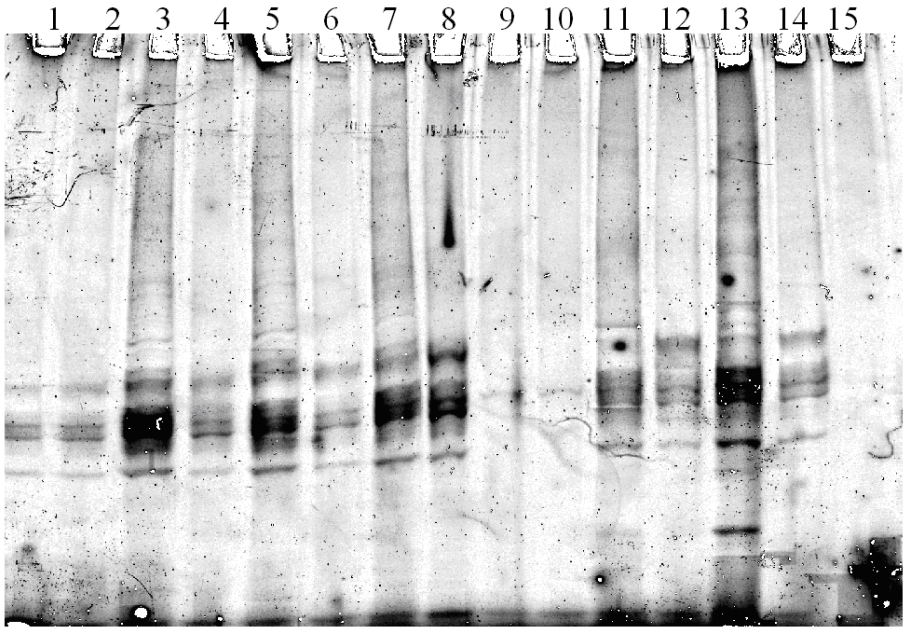

Figure 16. One-dimensional gel electrophoresis of fluorescently-labeled caspases collected every two hours post infection from 0 h.p.i. to 12 h.p.i. Samples were run in pairs of infected (odd lanes through lane 13) and non-infected (even lanes) from 0 h.p.i. (left) to 12 h.p.i. (right). Lane 15 is blank. Lanes 9 and 10 (8 h.p.i.) can be explained for their lack of fluorescently labeled proteins due to a mislabeling of sample vials.

In an attempt to identify the proteins labeled with the pan-caspase FLICA probe, labeled cells were analyzed on a two-dimensional gel. Cells were infected, labeled, and harvested as above. Infected and non-infected cells were both labeled and un-labeled at 0 and 12 h.p.i., resulting in eight total samples. Cells pellets underwent three freeze-thaw cycles of 15 minutes per environment at -80ºC and room temperature. Cell pellets were solublized in 300 μL Chaps-Urea buffer with 40 mM DTT and 5 μL DNase-RNase by gentle pipetting followed by tumbling at room temperature for 2 hours. Samples were

spun at 15,000 rpm for 10 minutes at 18 ºC to collect insoluble proteins. For each sample, 280 µL of the supernatant was transferred to a new tube and five volumes of ice-cold acetone were added. Samples were left at -80ºC for 3 hours to precipitate the protein. Samples were spun at 15,000 rpm for 10 minutes at 18 ºC to collect the protein pellet. The acetone was removed and the pellets were placed in a hood for 15 minutes to air dry.

Protein pellets were re-suspended in 100 uL Chaps-Urea buffer by tumbling at room temperature for 1 hour. Protein measurements were determined by a Bradford Assay, and protein concentrations averaged around 2.6 µg/µL. To 200 ug of each sample 2 uL DNase-RNase, 40 mM DTT, and 0.5% 3-11 NL ampholites were added. Chaps-Urea buffer was added to a total volume of 460 µL. Samples were centrifuged at 15,000 rpm for 10 minutes at 18 ºC to pellet any insoluble proteins remaining.

Samples were focused on a 3-11 non-linear, 24 cm IEF gel strip with an IPGphor until the focusing reached 45000 total Volt-hours. IEF strips were reduced with 10 mg/mL DTT in an equilibration buffer followed by modification with 25 mg/mL IAA. Strips were loaded onto 12.5% polyacrylamide gels and covered with 0.5% agarose. Gels were loaded into an Ettan Dalt II System and run at 150 constant volts for 15 hours. Gels were briefly washed in dH_2O before being imaged with a fluorescent scanner.

Gels were imaged using the Typhoon scanner using the 532/610 filter set (Figure 17). Cells exposed to the virus for 5 minutes (B) showed similar levels of FLICA labeling as the non-infected cells at 0 and 12 h.p.i. (A and C). Cells infected for 12 hours show an increase in intensity of fluorescently-labeled proteins (D). These gels indicate that the FLICA probe is labeling four distinct groups of proteins (E), each group characterized by

molecular weight and containing several proteins at different pI values. These trains are indicative of post-translational modifications.

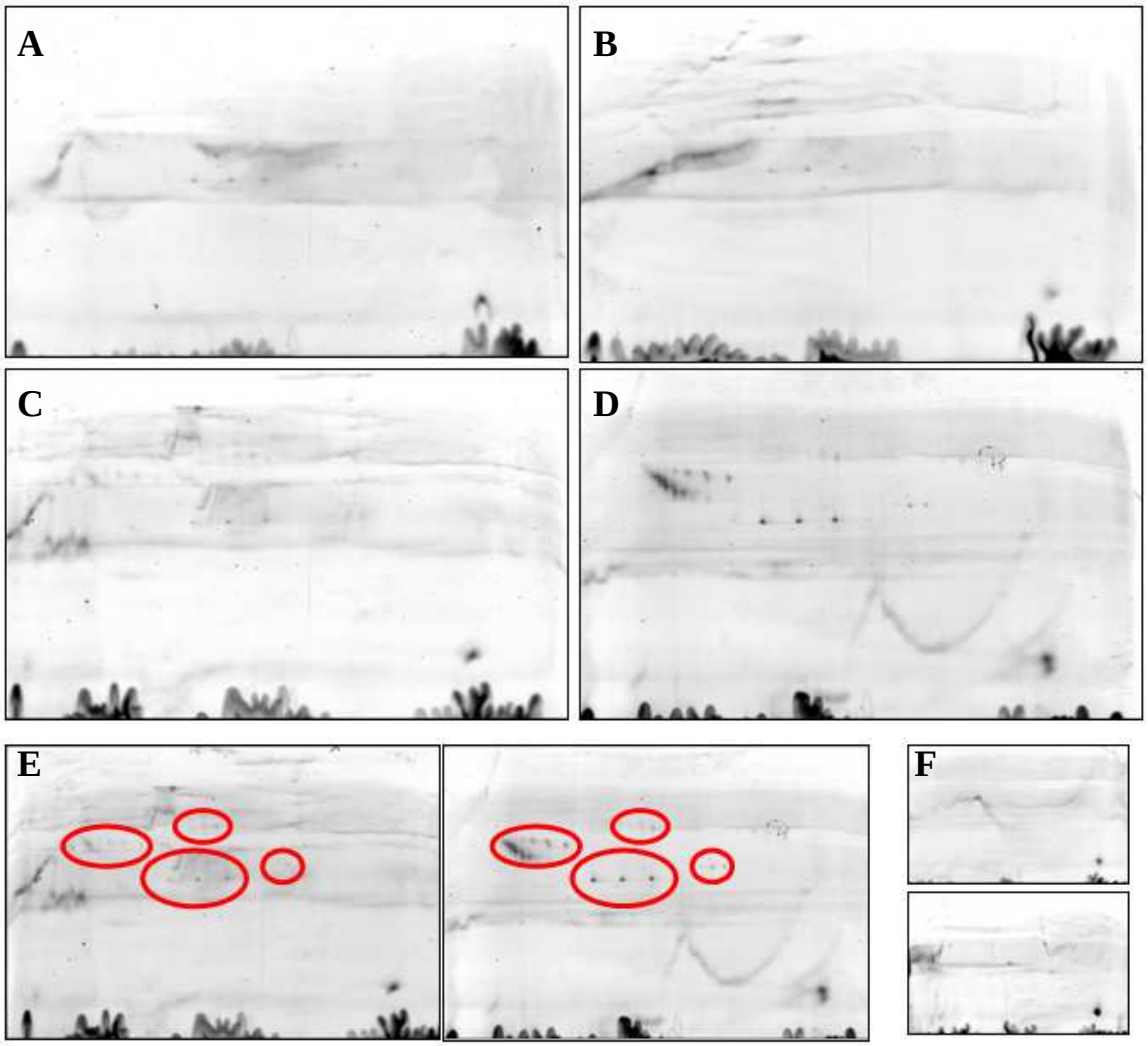

Figure 17. Fluorescent scanned 2D gels of pan-caspase, FLICA-labeled proteins in infected (B and D) and non-infected (A and C) RAW 264.7 cells at 1 h.p.i. (A and B) and 12 h.p.i. (C and D). E is highlighted proteins stained with FLICA at 12 h.p.i. in infected (right) and non-infected (left) RAW 264.7 cells. F illustrates a basic, low molecular weight, naturally fluorescing, non-FLICA labeled protein in the infected (bottom) and non-infected (top) RAW 264.7 cells 12 h.p.i.

Quantifying Caspase Activity

Caspase activity was also quantitatively analyzed using the FLICA-based probes in a fluorimetric assay described in the FLICA manual. Activity levels for caspases 2, 3/7, 8, and 9 were quantified with FLICA probes in addition to the total caspase activity indicated from the pan-caspase FLICA probe. Probes included FAM-VDVAD-fmk (caspase-2), FAM-DEVD-fmk (caspase-3/7), FAM-LETD-fmk (caspase-8), FAM-LEHD-fmk (caspase-9) and SR-VAD-fmk (pan-caspase). A fluormetric plate reader was used to measure the relative fluorescent units (RFUs) per sample at 1, 5, 9, and 13 hours post infection.

Cells were seeded in 2.0 mL of DMEM at a density of 2×10^6 cells per well in a 6-well plate and incubated at 37° C overnight. At 12, 8, 4, and 0 hours prior to labeling media were aspirated and replaced with fresh DMEM for non-infected cells or DMEM plus virus at an MOI of 0.5 for infected cells. Cells were scraped and harvested into 1.5 mL tubes 12 hours after the first inoculation. Cells were pelleted via centrifugation at 4,000 rpm for 10 minutes. The supernatant was discarded and 300 μL of the appropriate 1x FLICA probe in DMEM was added to an infected and a non-infected cell pellet for each time point. Pellets were re-suspended by vortexing and incubated at 37° C for 1 hour with two brief vortexes to ensure adequate mixing for labeling. Samples were washed with 1.0 mL of a 1x wash buffer diluted in PBS and centrifuged at 4,000 rpm for 5 minutes; the supernatant was aspirated and the wash was repeated. The pellets were re-suspended in 400 μL of PBS. Each sample was thoroughly mixed and 100 μL-aliquots were plated in triplicate in a 96-well plate.

Sample fluorescence was measured with a fluorimetric plate reader. Pan-caspase samples were measured with the 535/590 filter set, while all other samples were measured with the 490/535 filter set. Relative fluorescent units (RFUs) were recorded for each sample and average infected RFUs were normalized as a percentage of their control's average RFUs (Figure 18).

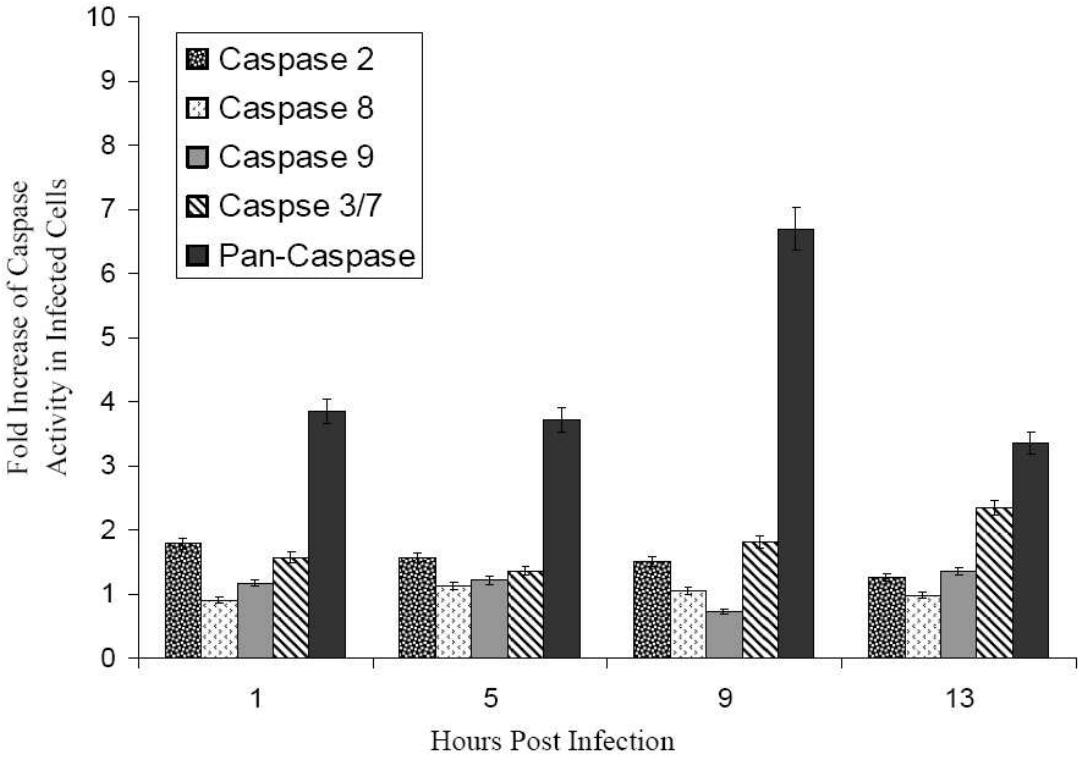

Figure 18. Caspase activity increases with MNV infection in RAW 264.7 cells. Caspase activity was fluorimetrically quantified in infected and non-infected cells at 1, 5, 9, and 13 h.p.i. using FLICA labeling. Relative light units (RFUs) are shown as the percent increase of signal in infected cells over the non-infected cells. Caspase 2 activity consistently decreases over time, while caspase 3/7 activity increases. The pan-caspase probe has a drastically increased signal at 9 h.p.i., which does not appear to result from a specific caspase.

In infected cells there is a clear increase in caspase activity. At each time point caspases 2 and 3/7 have increased activity. Caspase-2 activity decreases over time, while

caspase-3/7 increases its RFUs to over 200-percent of its non-infected counterpart at 13 h.p.i. Caspase-8 activity barely increases above the non-infected levels and caspase-9 fluctuates in relative activity, although it has a fairly significant increase in activity at 13 h.p.i. The pan-caspase activity levels in the infected cells are significantly increased when compared to the non-infected cells, which is only surprising when compared to the percent increases in activity of the other probed caspases. Some of the pan-caspase FLICA signal can potentially be contributed to non-probed caspases (1, 4, 6, 10, and 13), although there is a possibility that some non-specific labeling is happening with this probe, as evidence in the literature suggests that z-VAD-fmk binds to other cysteine proteases [136,137], specifically cathepsins [138].

Due to the excessive pan-caspase labeling, it was necessary to determine what proteins were being labeled by the caspase tag. A biotin-conjugated tag, biotin-X-DEVD-fmk, was used to label active caspase and separate them from the total cell lystate with streptavidin beads; this probe is specific for caspases 3, 6, 7, 8 and 10. Bound proteins were then identified using LC-MS/MS.

Briefly, cells were grown and infected as previously mentioned. At 12 h.p.i. infected and non-infected cells were harvested, pelleted, and re-suspended in 1.0 mL of 10 μM biotin-labeled tag in DMEM. One non-infected cell pellet was re-suspended in PBS alone to serve as a control. Cells were allowed to incubate at 37° C for one hour, pelleted, and washed once with 1x wash buffer. Cells were homogenized in 200 μL PBS binding buffer (0.15 M NaCl, and 0.1% SDS). 0.15 μL streptavidin agarose resin were added to the cells and mixed at room temperature for three hours. The resin was washed with 1.0 mL of binding buffer four times. Cells were washed once in PBS and digested

with trypsin in PBS overnight at 37° C. Digested samples were run on the ESI-MS/MS for protein identification.

Both control samples (labeled and un-labeled) yielded primarily keratin contamination with the presence of a histone in the un-labeled control sample. The infected sample contained cathepsins B peptides, which corresponds to previous studies suggesting that caspase inhibitors are weak in specificity and often target cathepsins[45,138]. This lack of specificity may explain the seemingly up-regulated activity of caspases as early as 2 h.p.i. in the imaging studies (Figure 14). Cathepsin is a lysosomal cysteine proteinase activated upstream of the mitochondrial pathway during apoptosis. Caspase activation is downstream of the mitochondrial release of cytochrome c, which has been shown to occur after 8 h.p.i. during FCV infection[33]. These results suggest that early detection of caspase activity may actually be detection of cathepsin activity.

CASPASE-INDEPENDENT CELL DEATH: APOPTOSIS OR NECROSIS?

Background

Apoptosis is mediated through a series of interconnecting pathways involving caspases. In the previous chapter it was noted that caspase activity increases with the presence of the MNV and that cells undergo caspase-mediated apoptosis. These data beg the question: What happens to infected cells if the caspase pathway is blocked? This question can be investigated by infecting the cells in the presence of a pan-caspase inhibitor.

By blocking caspase activation, several pathways resulting in apoptosis are effectively nullified. For example, blocking caspase-3 prevents DNA fragmentation, a prominent component of apoptosis, from occurring. Because caspase-3 is activated by initiator caspases, such as caspase-2, -8, and -9, it can also be indirectly blocked. There are many components of apoptosis that can be monitored and inhibited; however, for these studies only the effects of caspases will be explored.

The Boc-D(OMe)-fmk inhibitor was chosen as the caspase inhibitor because it is a pan-caspase inhibitor, is membrane permeable, and is irreversible upon binding. O-methylating the aspartic acid residue increases the membrane permeability of the probe. This inhibitor prevents the pro-caspases from being cleaved into their active forms by covalently binding to caspase proteases, thus indirectly blocking caspase activation.

The following experiments focus on comparing caspase-independent cell death with caspase-dependent cell death in RAW 264.7 cells infected with MNV. Primarily,

cell viability and effects on apoptosis were monitored through cell imaging. A comparison of cells infected in the presence and absence of the pan-caspase inhibitor, Boc-D(OMe)-fmk, was made with respect to the changes in cell morphology, DNA fragmentation, and cellular membrane permeability.

DNA Fragmentation

DNA fragmentation is one of the defining components of apoptosis and is initiated through caspase-3 activation. DNA fragmentation was confirmed in MNV-infected cells by gel electrophoresis according to methods of Zhu and Wang [30]. Briefly, 8 x 10^6 infected and non-infected cells were scraped and pelleted 6, 12, 18, and 24 h.p.i. Cells were washed twice with ice-cold PBS, which was replaced with 20 μL of lysis buffer (10 mM Tris, pH 7.4, 100 mM NaCl, 25 mM EDTA, and 1% sarkosyl) and 8 μL of 5 μg/mL proteinase K and samples were incubated at 45° C for 2 hours. 2 μL of RNase were added per sample and samples were incubated at room temperature for an additional 2 hours. 4 μL of sample buffer (50% glycerol, 1 mM EDTA, pH 8.0, and 0.25% bromophenol blue) was added to each sample before loading it onto a 2% agarose gel with 0.5% ethidium bromide. The gel was run at 100 V for 1 hour and imaged (Figure 19).

The DNA of infected cells began fragmenting at 18 h.p.i. and was more obvious at 24 h.p.i. Non-infected cellular DNA remained whole at all time points, as did the infected cells at 6 and 12 h.p.i. These results support the previous caspase data, which suggests that cells infected with MNV undergo a capsase-mediated, apoptotic cell death.

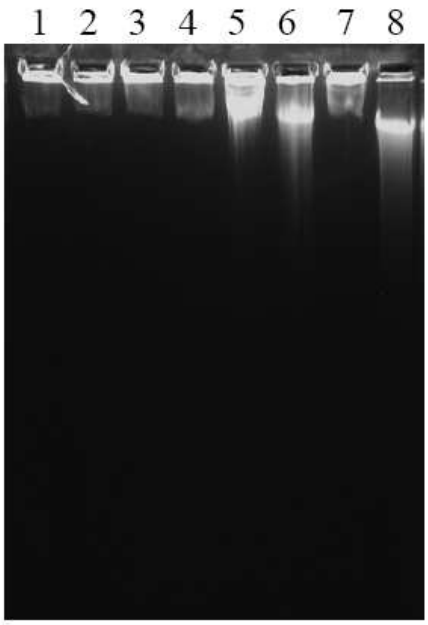

Figure 19. Apoptosis results in DNA fragmentation in virally infected cells. Infected (even lanes) and non-infected (odd lanes) cellular DNA was collected at 6, 12, 18, and 24 h.p.i. and analyzed on a 2% agarose gel. Cellular DNA remained intact in both infected and non-infected cells at 6 and 12 h.p.i. (lanes 1-4), while DNA fragmentation was visible in the infected cells at 18 and 24 h.p.i. (lanes 6 and 8) but not the non-infected cells (lanes 5 and 7).

Cell Viability

Cell viability was monitored in cells infected in the presence and absence of a pan-caspase inhibitor with respect to their non-infected counterparts. At 0, 12, 18, and 24 h.p.i. cell counts and percent viability were determined and non-contrast images were taken.

Cells were seeded in 1.0 mL DMEM at a density of 5×10^5 cells per well in four 12-well plates and left to incubate at 37° C overnight. DMEM was replaced with 0.5 mL DMEM plus 2.5 μL DMSO (control), DMEM with 100 μM Boc-D(OMe)-fmk (inhibitor control), DMEM with 2.5 μL DMSO and virus (MOI=0.5)(virus), DMEM with 100 μM

Boc-D(OMe)-fmk and virus (inhibitor virus). Each condition was repeated in triplicate for all four time points.

At each time point, cells were imaged using an inverted Nikon TE300 microscope at 200x and 400x magnifications. Cells were then scraped, collected, and diluted 1:1 with Trypan Blue. 10 μL of the stained cells were counted with a hemacytometer to determine the total cell counts and percent viability.

At 12 h.p.i. the percent cell viability differences were apparent between the infected samples with and without the inhibitor. Percent viability also sharply declined from 12 to 18 h.p.i. in the caspase-inhibited cells and fell below ten percent viability by 24 h.p.i. (Figure 20), while the non-inhibited infected cells remained above 60-70 percent viable during the same time.

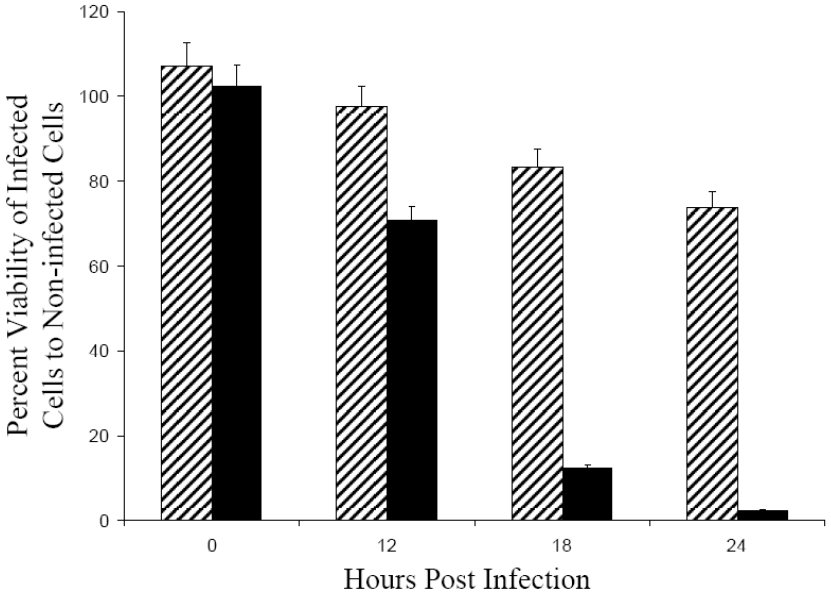

Figure 20. RAW 264.7 cell viability decreases more rapidly during MNV infection in the presence of a pan-caspase inhibitor, Boc-D-fmk (black), than in cells without the inhibitor (striped). The data are represented as the percent cell viability of the infected to non-infected cells.

By 18 h.p.i. there were clear morphological changes visualized with the microscope (Figure 21), which were also apparent at 24 h.p.i. (Figure 22). Cells infected in the presence of the inhibitor had a greater percentage of lifted cells and lacked extensive appendages that were present in the absence of the caspase inhibitor. By 24 h.p.i. the cell density in the non-inhibited infected cells sharply declined, possibly due to the cells breaking apart during apoptosis, while the inhibited cells remained intact.

In a separate but similar study (described below), cells were stained for chromatin condensation and membrane permeability. During this experiment several non-contrast images were taken of cells infected in the presence and absence of the pan-caspase inhibitor at 6, 12, 18, and 24 hours post infection (Figure 23). The primary difference between these images and those taken in the previous experiment is that the cells were scraped from their well and went through a series of washes and staining before being imaged on a glass slide with a coverslip. In the previous experiments, cells were imaged directly in their tissue culture plates. This difference explains the lack of flat, adherent cells with appendages that were visualized in Figure 21. The cell images provide examples of several morphological changes. Cellular membrane blebbing, swelling, and cytoplasmic leaking are evident in cells infected in the presence of the caspase inhibitor. This series of changes is characteristic of a necrotic cell death versus an apoptotic death. In the non-caspase inhibited cells, blebbing occurs at 6 h.p.i., after which the cells begin to shrink and break apart into apoptotic bodies. In general, cells infected in the presence of the inhibitor tend to swell and bulge, while those infected without the inhibitor shrink and break apart. These morphological changes suggest that while infected cells in the

absence of the caspase inhibitor undergo apoptosis, cells infected with the caspase inhibitor may undergo necrosis.

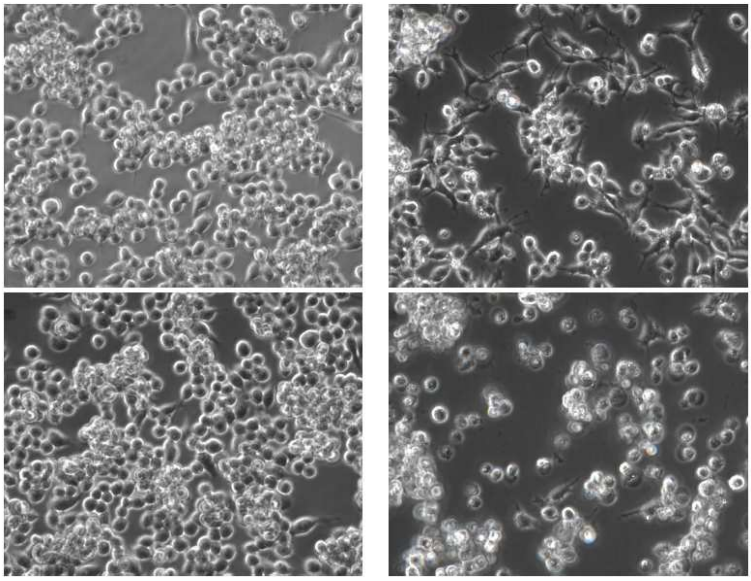

Figure 21. Cell morphology 18 hours post infection of caspase-inhibited (bottom) and caspase-uninhibited cells (top). Non-infected cells (left) were morphologically unaffected by the presence of the caspase inhibitor, Boc-D(MeO)-fmk. Morphological differences were present between cells infected in the presence and absence of the caspase inhibitor (right).

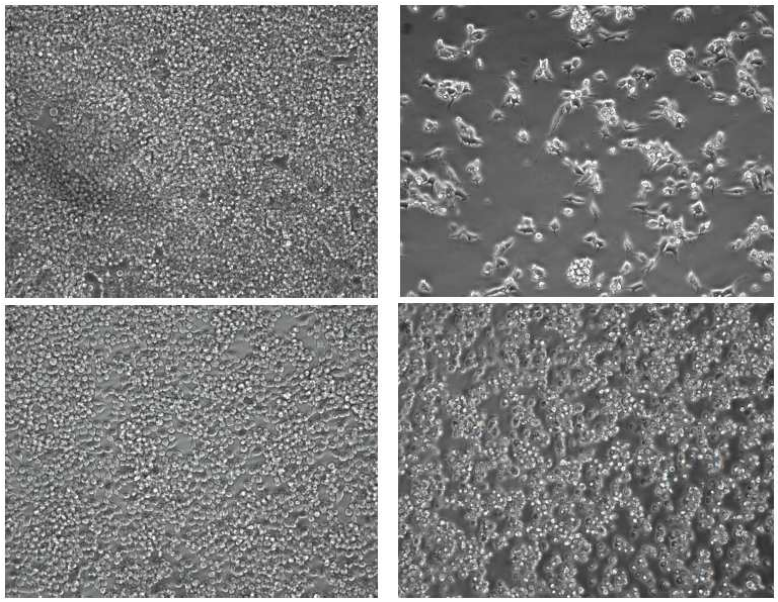

Figure 22. Infected (right) and non-infected (left) cells in the presence (bottom) or absence (top) of the pan-caspase inhibitor, Boc-D(OMe)-fmk at 24 h.p.i.

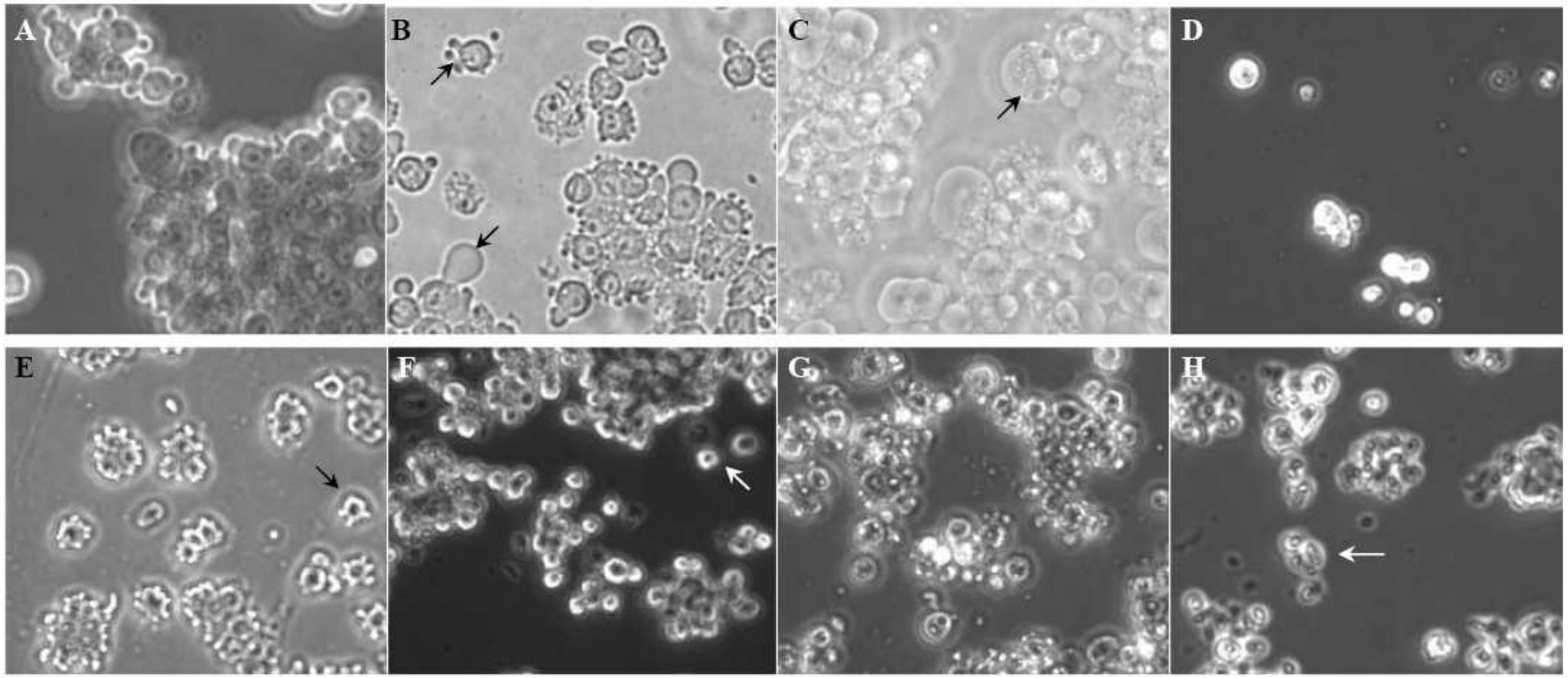

Figure 23. Cell morphology changes with viral infection in the presence (A-D) and absence (E-H) of a pan-caspase inhibitor, Boc-D(MeO)-fmk. Cell images were taken at 6, 12, 18, and 24 h.p.i. (left to right). In cells infected with the inhibitor (A-D), their morphology goes through a series of changes including membrane blebbing and expanding (arrows panel B) and cellular swelling (arrow panel C). Cells undergoing caspase-mediated cell death show signs of apoptosis, such as membrane blebbing (arrow panel E), cell shrinkage (arrow panel F), and cellular fragmentation (arrow panel H).

Through these experiments it was evident that caspase-independent cell death differed from non-inhibited cell death in the presence of the virus, thus indicating that caspases may be important in the normal progression of the virus.

Cellular Staining

Apoptosis can be determined through propidium iodide and Hoechst staining, and DNA laddering [139] [140] [141]. Propidium iodide (PI) is commonly used to detect dead cells, as it is membrane impermeable. During apoptosis cells lose their membrane integrity, which allows the dye to permeate into the cell. Once inside the cell, PI can bind to the cellular nucleic acids and will increase in fluorescence upon doing so; thus, apoptotic cells will fluoresce an intense red, necrotic cells may become a diffuse red, and healthy cells will remain unstained. Hoechst staining is commonly used as a more membrane permeable substitute for DAPI; both bind to DNA and are used to stain the nucleus. When DNA is condensed due to fragmentation during apoptosis, the nucleus stains an intense blue. When the DNA is non-fragmented, the nucleus remains a diffuse blue. Since DNA fragmentation is a vital part of apoptosis, Hoechst staining is often used to differentiate between apoptotic and non-apoptotic cells. By combining these two stains, cells can easily be characterized as apoptotic or non-apoptotic; however, concluding that a cell is necrotic is less specific.

Cells infected in the presence and absence of the pan-caspase inhibitor, Boc-D(OMe)-fmk, were stained with PI and Hoechst to determine if apoptosis was occurring. Cells were stained as described by Pelfry et al. [140].

Cells were seeded at a density of 5 x 10^5 cells per well in 1.0 mL DMEM in 12-well plates and incubated overnight at 37° C. Media were replaced with 0.5 mL DMEM plus virus at an MOI of 1 for infected cells and 100 μM Boc-D(OMe)-fmk for caspase-inhibited cells. Cells were infected and harvested at 6, 12, 18, and 24 h.p.i. for PI and Hoechst staining.

Cells were scraped, collected into 1.5 mL tubes, and centrifuged at 4000 rpm to pellet. The supernatant was aspirated and replaced with 250 μL of 1.6 μg/mL Hoechst stain diluted in sterile PBS. Cells were gently mixed with a 1000 μL-volume pipette tip before being incubated at 37° C for 15 minutes. 5 μL of 250 μg/mL PI stain was added to the cells and allowed to briefly incubate before centrifugation at 4000 rpm for 5 minutes. The supernatant was discarded, and the cells were gently re-suspended in 20 μL of sterile PBS. 10 μL of cell suspension were plated onto a glass slide with a cover slip in preparation for imaging.

Cells were imaged on a Nikon TE300 inverted microscope. Filter sets were used to visualize the PI and Hoechst stain. Digital cell images were taken at 400x magnification with each filter set and the images were merged using OneSpot software (Figure 24, Figure 25, Appendix B, and Appendix C).

Images were analyzed using ImageJ and a cell counter plug-in. Each image was individually analyzed for total cell counts and intensely stained cells. Hoechst-stained cells were counted and differentiated as having diffusely stained or intensely stained nuclei for each image. PI-stained cells were counted for the total number of membrane permeable cells per image.

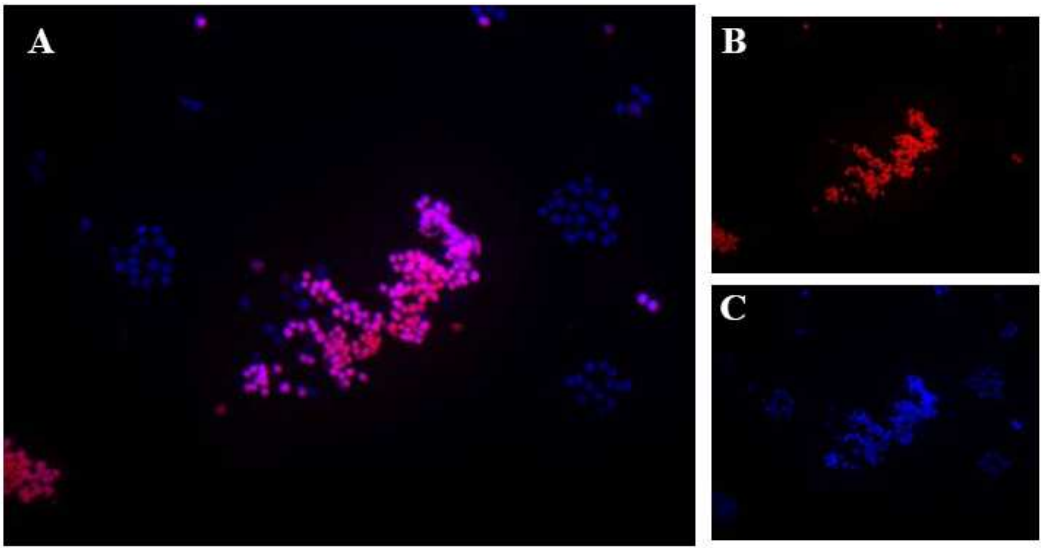

Figure 24. Cells stained with propidium iodide and Hoechst stains 18 hours post infection (A). Cells stained bright red with propidium iodide indicate membrane permeability (B), while those stained an intense blue with Hoechst stain have condensed chromatin (C), which is indicative of apoptosis. Faint blue cells are healthy, purple cells are apoptotic, and red cells are membrane permeable without chromatin condensation.

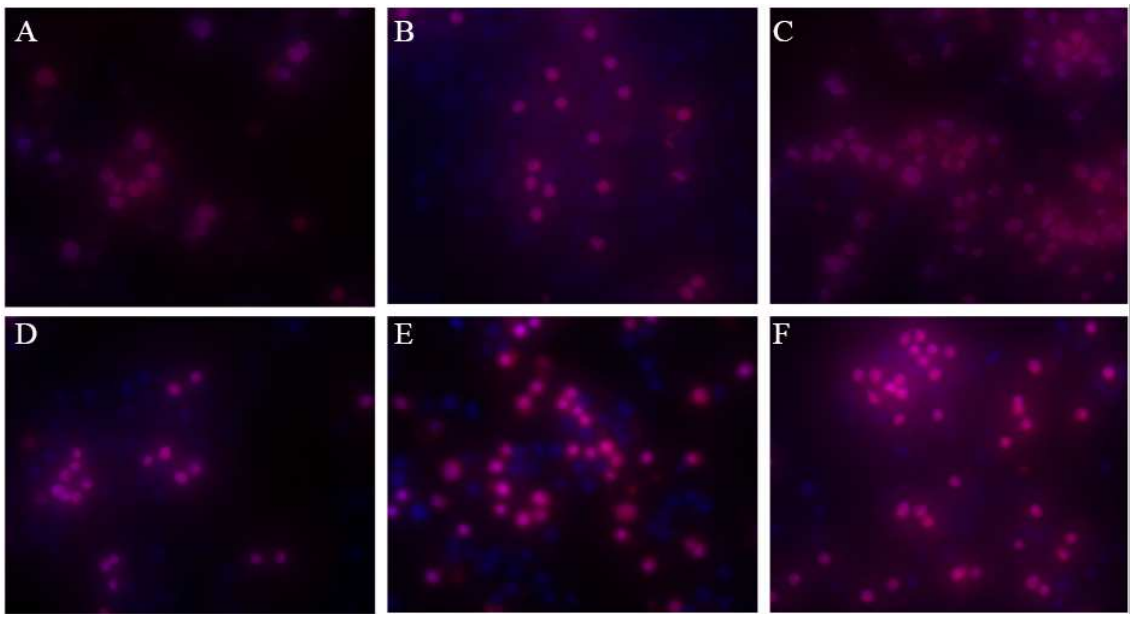

Figure 25. Multiplex staining with propidium iodide (PI) and Hoechst stains in virally infected cells in the presence (top) and absence (bottom) of a pan-caspase inhibitor, Boc-D(OMe)-fmk. Cell images were taken at 6, 12, and 18 h.p.i. (left to right). Cells stained with PI appear diffuse pink in necrotic cells (A-C) and bright pink in apoptotic cells (D-F). Hoechst stain appears bright blue in cells with condensed chromatin, indicating apoptosis.

The percentage of cells with condensed chromatin was normalized to the control cells' percentages for each time point to determine the virally induced changes in chromatin condensation. Cells infected in the absence of the caspase inhibitor showed a gradual increase in Hoechst staining over the 24 hours when compared with the non-infected cells, having 70 percent more apoptotic cells than the control at 24 h.p.i. Cells infected in the presence of the inhibitor showed a minimal increase in staining above its control, with less than a 10 percent increase at any time point (Figure 26). These data indicate that DNA fragmentation, which results in chromatin condensation, is minimal in cells infected in the presence of a pan-caspase inhibitor but extensive in cells infected without the inhibitor.

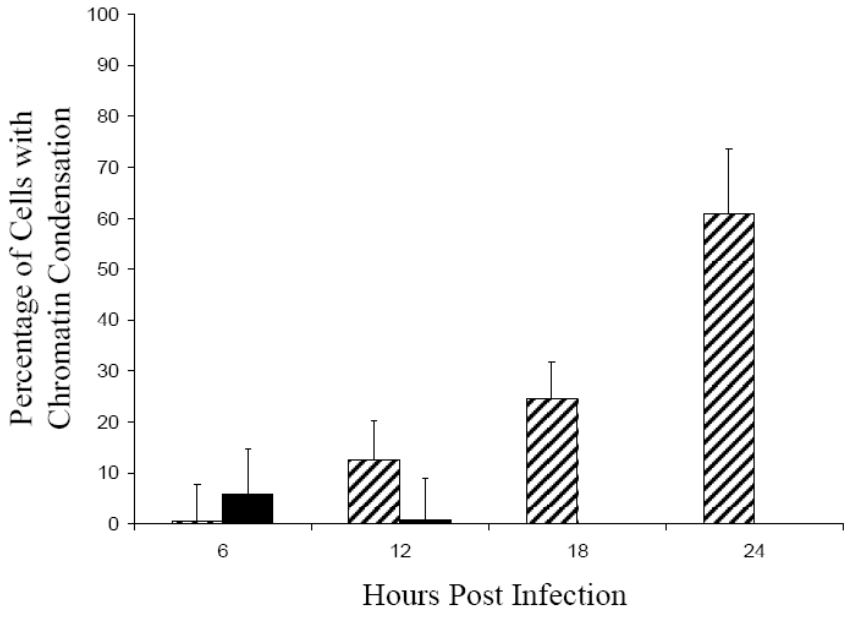

Figure 26. Percentage of infected cells normalized against non-infected cells with condensed chromatin staining at 6, 12, 18, and 24 h.p.i. Cells were infected in the presence (black) and absence (striped) of a pan-caspase inhibitor, Boc-D(MeO)-fmk. Only samples infected in the absence of the caspase inhibitor show an increase in chromatin condensation. Asterisk indicates a higher percentage of chromatin staining in the control sample.

Because PI is membrane impermeable, it can be concluded that cells stained red have lost their membrane integrity, which is an indicator of cell death. The percentage of infected cells stained with PI was determined and was normalized to the control cells' values (Figure 27). While cells infected in both the presence and absence of the caspase inhibitor showed signs of membrane permeability, cells infected with the inhibitor reveal a more drastic shift to membrane permeability than those infected without the inhibitor. These data suggest a more controlled cell death in cells undergoing caspase-mediated cell death versus cells undergoing caspase-independent cell death.

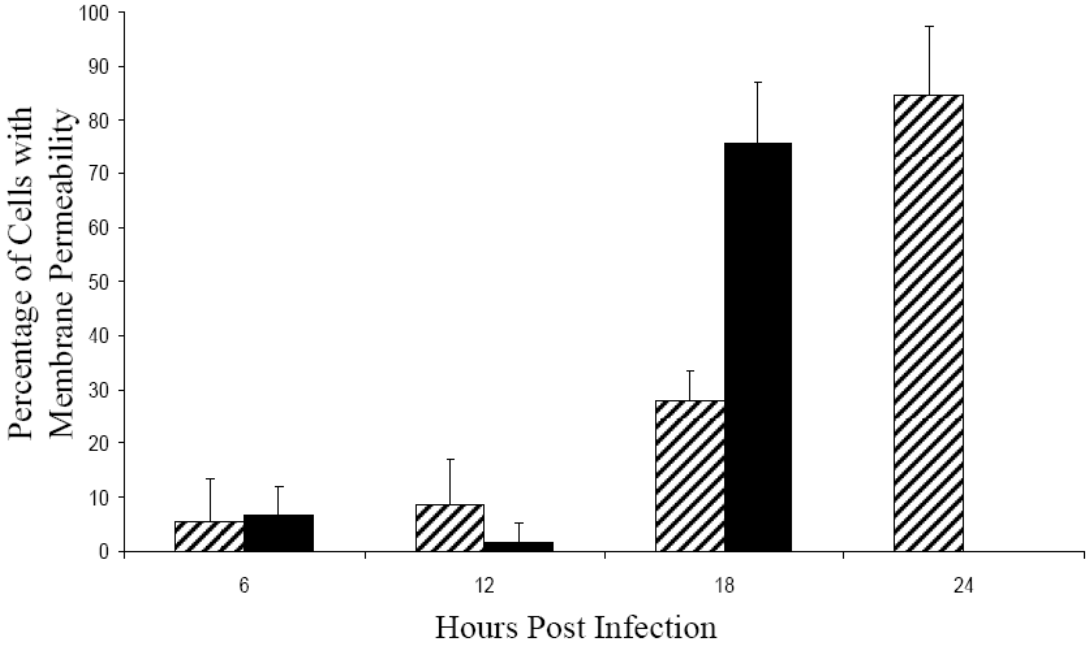

Figure 27. Percentage of infected cells normalized against non-infected cells with propidium iodide staining at 6, 12, 18, and 24 h.p.i. Cells were infected in the presence (black) and absence (striped) of a pan-caspase inhibitor, Boc-D(MeO)-fmk. Cells infected in the absence of the inhibitor steadily become more permeable, while cells infected in the presence of the pan-caspase inhibitor become more permeable between 12 and 18 h.p.i.

When combined, the cell morphology images and the PI and Hoechst stains convincingly suggest that cells infected in the presence of a pan-caspase inhibitor, Boc-

D(OMe)-fmk, undergo a different type of cell death than cells infected in the absence of the inhibitor. In the absence of the caspase-inhibitor infected cells show morphological signs indicative of apoptosis, have a high percentage of cells with chromatin condensation, and greater than 80 percent of the cells are membrane permeable. In the presence of the caspase inhibitor, infected cells show morphological signs of necrosis and have a minimal percentage of cells with chromatin condensation; however, these cells do have a more pronounced transition from membrane impermeability to membrane permeability. These findings provide evidence that RAW 264.7 cells infected with MNV naturally undergo caspase-mediated apoptosis, and that cells infected in the presence of the pan-caspase inhibitor Boc-D(OMe)-fmk undergo a modified cell death more closely resembling necrosis.

CONCLUDING REMARKS

In the past five years there has been significant insight toward understanding human norovirus infections through the MNV model system. This is the first global perspective of the proteomic changes that occur in the host cells during norovirus infection. The conclusion from these 2D-DIGE and ABPP experiments is threefold: 1) several apoptotic-related proteins are regulated at 4 and 12 h.p.i., most of which are structurally significant or are connected to mitochondrial release of cytochrome c; 2) caspases, which are key modulators of apoptosis, are activated during infection; and 3) caspase-independent cell death, induced in the presence of a pan-caspase inhibitor, is markedly different than the natural virally induced cell death. Through these techniques there is convincing evidence that cells infected with MNV undergo caspase-mediated apoptosis and inhibiting caspase activity significantly alters the natural mode of cell death.

Future studies should continue characterizing caspase-independent cell death as presented in this paper. Using Northern and Western blotting techniques, the production of viral RNA and capsid protein could be monitored in response to caspase inhibition. Specifically, the virus's ability to replicate in the absence of caspase-3 would determine if caspase-3 is required for polyprotein cleavage as Sosnovtsev et al. proposed in 2006[39].

Also, further investigation of the relationship between STAT1 and caspases with cell death should be conducted. STAT1 is essential in the innate immune response to norovirus infection, as infection is fatal in STAT1-deficient mice. Recent studies have

shown a positive correlation between STAT1 and caspase expression levels[142,143]. Specifically, STAT1 increases cytochrome c release from the mitochondria, increasing caspase-3 levels and apoptosis. In STAT1-defficeint mice this correlation may negatively affect the natural apoptotic process during infection. Furthermore, investigation into the effects of ROS activation during infection should be conducted. Due to the correlation of caspases and STAT1 with ROS, investigating the mechanisms of ROS activation during MNV infection may help characterize the differences between caspase-dependent and caspase-independent cell death.

REFERENCES CITED

1. Wobus, CE, Thackray, LB and Virgin, HWt, (2006) Murine norovirus: a model system to study norovirus biology and pathogenesis. J Virol 80: 5104-12.

2. Phan, TG, Kaneshi, K, Ueda, Y, Nakaya, S, Nishimura, S, Yamamoto, A et al., (2007) Genetic heterogeneity, evolution, and recombination in noroviruses. J Med Virol 79: 1388-400.

3. Thackray, LB, Wobus, CE, Chachu, KA, Liu, B, Alegre, ER, Henderson, KS et al., (2007) Murine noroviruses comprising a single genogroup exhibit biological diversity despite limited sequence divergence. J Virol 81: 10460-73.

4. Hardy, ME, (2005) Norovirus protein structure and function. FEMS Microbiol Lett 253: 1-8.

5. Daughenbaugh, KF, Wobus, CE and Hardy, ME, (2006) VPg of murine norovirus binds translation initiation factors in infected cells. Virol J 3: 33.

6. Kuyumcu-Martinez, M, Belliot, G, Sosnovtsev, SV, Chang, KO, Green, KY and Lloyd, RE, (2004) Calicivirus 3C-like proteinase inhibits cellular translation by cleavage of poly(A)-binding protein. J Virol 78: 8172-82.

7. Chakravarty, S, Hutson, AM, Estes, MK and Prasad, BV, (2005) Evolutionary trace residues in noroviruses: importance in receptor binding, antigenicity, virion assembly, and strain diversity. J Virol 79: 554-68.

8. Xia, M, Farkas, T and Jiang, X, (2007) Norovirus capsid protein expressed in yeast forms virus-like particles and stimulates systemic and mucosal immunity in mice following an oral administration of raw yeast extracts. J Med Virol 79: 74-83.

9. Bertolotti-Ciarlet, A, White, LJ, Chen, R, Prasad, BV and Estes, MK, (2002) Structural requirements for the assembly of Norwalk virus-like particles. J Virol 76: 4044-55.

10. Ettayebi, K and Hardy, ME, (2003) Norwalk virus nonstructural protein p48 forms a complex with the SNARE regulator VAP-A and prevents cell surface expression of vesicular stomatitis virus G protein. J Virol 77: 11790-7.

11. Hardy, ME, Crone, TJ, Brower, JE and Ettayebi, K, (2002) Substrate specificity of the Norwalk virus 3C-like proteinase. Virus Res 89: 29-39.

12. Nakamura, K, Someya, Y, Kumasaka, T, Ueno, G, Yamamoto, M, Sato, T et al., (2005) A norovirus protease structure provides insights into active and substrate binding site integrity. J Virol 79: 13685-93.

13. Xi, JN, Graham, DY, Wang, KN and Estes, MK, (1990) Norwalk virus genome cloning and characterization. Science 250: 1580-3.

14. Lochridge, VP, Jutila, KL, Graff, JW and Hardy, ME, (2005) Epitopes in the P2 domain of norovirus VP1 recognized by monoclonal antibodies that block cell interactions. J Gen Virol 86: 2799-806.

15. LoBue, AD, Lindesmith, L, Yount, B, Harrington, PR, Thompson, JM, Johnston, RE et al., (2006) Multivalent norovirus vaccines induce strong mucosal and systemic blocking antibodies against multiple strains. Vaccine 24: 5220-34.

16. Parker, TD, Kitamoto, N, Tanaka, T, Hutson, AM and Estes, MK, (2005) Identification of Genogroup I and Genogroup II broadly reactive epitopes on the norovirus capsid. J Virol 79: 7402-9.

17. Souza, M, Costantini, V, Azevedo, MS and Saif, LJ, (2007) A human norovirus-like particle vaccine adjuvanted with ISCOM or mLT induces cytokine and antibody responses and protection to the homologous GII.4 human norovirus in a gnotobiotic pig disease model. Vaccine 25: 8448-59.

18. Duizer, E, Schwab, KJ, Neill, FH, Atmar, RL, Koopmans, MP and Estes, MK, (2004) Laboratory efforts to cultivate noroviruses. J Gen Virol 85: 79-87.

19. White, LJ, Ball, JM, Hardy, ME, Tanaka, TN, Kitamoto, N and Estes, MK, (1996) Attachment and entry of recombinant Norwalk virus capsids to cultured human and animal cell lines. J Virol 70: 6589-97.

20. Karst, SM, Wobus, CE, Lay, M, Davidson, J and Virgin, HWt, (2003) STAT1-dependent innate immunity to a Norwalk-like virus. Science 299: 1575-8.

21. Wobus, CE, Karst, SM, Thackray, LB, Chang, KO, Sosnovtsev, SV, Belliot, G et al., (2004) Replication of Norovirus in cell culture reveals a tropism for dendritic cells and macrophages. PLoS Biol 2: e432.

22. Cannon, JL, Papafragkou, E, Park, GW, Osborne, J, Jaykus, LA and Vinje, J, (2006) Surrogates for the study of norovirus stability and inactivation in the environment: aA comparison of murine norovirus and feline calicivirus. J Food Prot 69: 2761-5.

23. Bae, J and Schwab, KJ, (2008) Evaluation of murine norovirus, feline calicivirus, poliovirus, and MS2 as surrogates for human norovirus in a model of viral persistence in surface water and groundwater. Appl Environ Microbiol 74: 477-84.

24. Baert, L, Wobus, CE, Van Coillie, E, Thackray, LB, Debevere, J and Uyttendaele, M, (2008) Detection of murine norovirus 1 by using plaque assay, transfection

assay, and real-time reverse transcription-PCR before and after heat exposure. Appl Environ Microbiol 74: 543-6.

25. Lee, J, Zoh, K and Ko, G, (2008) Inactivation and UV/TiO2 Disinfection of Murine Norovirus under Various Environmental Conditions. Appl Environ Microbiol.

26. Kingsley, DH, Holliman, DR, Calci, KR, Chen, H and Flick, GJ, (2007) Inactivation of a norovirus by high-pressure processing. Appl Environ Microbiol 73: 581-5.

27. Hsu, CC, Riley, LK and Livingston, RS, (2007) Molecular characterization of three novel murine noroviruses. Virus Genes 34: 147-55.

28. Hsu, CC, Riley, LK, Wills, HM and Livingston, RS, (2006) Persistent infection with and serologic cross-reactivity of three novel murine noroviruses. Comp Med 56: 247-51.

29. Lochridge, VP and Hardy, ME, (2007) A single-amino-acid substitution in the P2 domain of VP1 of murine norovirus is sufficient for escape from antibody neutralization. J Virol 81: 12316-22.

30. Zhu, N and Wang, Z, (1997) An assay for DNA fragmentation in apoptosis without phenol/chloroform extraction and ethanol precipitation. Anal Biochem 246: 155-8.

31. Majno, G and Joris, I, (1995) Apoptosis, oncosis, and necrosis. An overview of cell death. Am J Pathol 146: 3-15.

32. Nagaleekar, VK, Tiwari, AK, Kataria, RS, Bais, MV, Ravindra, PV and Kumar, S, (2007) Bluetongue virus induces apoptosis in cultured mammalian cells by both caspase-dependent extrinsic and intrinsic apoptotic pathways. Arch Virol 152: 1751-6.

33. Natoni, A, Kass, GE, Carter, MJ and Roberts, LO, (2006) The mitochondrial pathway of apoptosis is triggered during feline calicivirus infection. J Gen Virol 87: 357-61.

34. Thornberry, NA, Rano, TA, Peterson, EP, Rasper, DM, Timkey, T, Garcia-Calvo, M et al., (1997) A combinatorial approach defines specificities of members of the caspase family and granzyme B. Functional relationships established for key mediators of apoptosis. J Biol Chem 272: 17907-11.

35. Hay, S and Kannourakis, G, (2002) A time to kill: viral manipulation of the cell death program. J Gen Virol 83: 1547-64.

36. Barber, GN, (2001) Host defense, viruses and apoptosis. Cell Death Differ 8: 113-26.

37. Roulston, A, Marcellus, RC and Branton, PE, (1999) Viruses and apoptosis. Annu Rev Microbiol 53: 577-628.

38. Sosnovtsev, SV, Prikhod'ko, EA, Belliot, G, Cohen, JI and Green, KY, (2003) Feline calicivirus replication induces apoptosis in cultured cells. Virus Res 94: 1-10.

39. Sosnovtsev, SV, Belliot, G, Chang, KO, Prikhodko, VG, Thackray, LB, Wobus, CE et al., (2006) Cleavage map and proteolytic processing of the murine norovirus nonstructural polyprotein in infected cells. J Virol 80: 7816-31.

40. Liu, Y, Patricelli, MP and Cravatt, BF, (1999) Activity-based protein profiling: the serine hydrolases. Proc Natl Acad Sci U S A 96: 14694-9.

41. Kidd, D, Liu, Y and Cravatt, BF, (2001) Profiling serine hydrolase activities in complex proteomes. Biochemistry 40: 4005-15.

42. Schmidinger, H, Hermetter, A and Birner-Gruenberger, R, (2006) Activity-based proteomics: enzymatic activity profiling in complex proteomes. Amino Acids 30: 333-50.

43. Greenbaum, DC, Arnold, WD, Lu, F, Hayrapetian, L, Baruch, A, Krumrine, J et al., (2002) Small molecule affinity fingerprinting. A tool for enzyme family subclassification, target identification, and inhibitor design. Chem Biol 9: 1085-94.

44. van Swieten, PF, Maehr, R, van den Nieuwendijk, AM, Kessler, BM, Reich, M, Wong, CS et al., (2004) Development of an isotope-coded activity-based probe for the quantitative profiling of cysteine proteases. Bioorg Med Chem Lett 14: 3131-4.

45. Kato, D, Boatright, KM, Berger, AB, Nazif, T, Blum, G, Ryan, C et al., (2005) Activity-based probes that target diverse cysteine protease families. Nat Chem Biol 1: 33-8.

46. Gredmark, S, Schlieker, C, Quesada, V, Spooner, E and Ploegh, HL, (2007) A functional ubiquitin-specific protease embedded in the large tegument protein (ORF64) of murine gammaherpesvirus 68 is active during the course of infection. J Virol 81: 10300-9.

47. Saghatelian, A, Jessani, N, Joseph, A, Humphrey, M and Cravatt, BF, (2004) Activity-based probes for the proteomic profiling of metalloproteases. Proc Natl Acad Sci U S A 101: 10000-5.

48. Freije, JR and Bischoff, R, (2003) Activity-based enrichment of matrix metalloproteinases using reversible inhibitors as affinity ligands. J Chromatogr A 1009: 155-69.

49. Chan, EW, Chattopadhaya, S, Panicker, RC, Huang, X and Yao, SQ, (2004) Developing photoactive affinity probes for proteomic profiling: hydroxamate-based probes for metalloproteases. J Am Chem Soc 126: 14435-46.

50. Zhang, S, Chen, L, Kumar, S, Wu, L, Lawrence, DS and Zhang, ZY, (2007) An affinity-based fluorescence polarization assay for protein tyrosine phosphatases. Methods 42: 261-7.

51. Liang, F, Kumar, S and Zhang, ZY, (2007) Proteomic approaches to studying protein tyrosine phosphatases. Mol Biosyst 3: 308-16.

52. Kumar, S, Zhou, B, Liang, F, Wang, WQ, Huang, Z and Zhang, ZY, (2004) Activity-based probes for protein tyrosine phosphatases. Proc Natl Acad Sci U S A 101: 7943-8.

53. Sieber, SA, Mondala, TS, Head, SR and Cravatt, BF, (2004) Microarray platform for profiling enzyme activities in complex proteomes. J Am Chem Soc 126: 15640-1.

54. Fonovic, M, Verhelst, SH, Sorum, MT and Bogyo, M, (2007) Proteomics evaluation of chemically cleavable activity-based probes. Mol Cell Proteomics 6: 1761-70.

55. Ralph, P and Nakoinz, I, (1977) Antibody-dependent killing of erythrocyte and tumor targets by macrophage-related cell lines: enhancement by PPD and LPS. J Immunol 119: 950-54.

56. Raschke, WC, Baird, S, Ralph, P and Nakoinz, I, (1978) Functional macrophage cell lines transformed by Abelson leukemia virus. Cell 15: 261-7.

57. Gonzalez-Santiago, L, Alfonso, P, Suarez, Y, Nunez, A, Garcia-Fernandez, LF, Alvarez, E et al., (2007) Proteomic analysis of the resistance to aplidin in human cancer cells. J Proteome Res 6: 1286-94.

58. Kisby, GE, Standley, M, Park, T, Olivas, A, Fei, S, Jacob, T et al., (2006) Proteomic analysis of the genotoxicant methylazoxymethanol (MAM)-induced changes in the developing cerebellum. J Proteome Res 5: 2656-65.

59. Roelens, SA, Beck, V, Aerts, G, Clerens, S, Vanden Bergh, G, Arckens, L et al., (2005) Neurotoxicity of polychlorinated biphenyls (PCBs) by disturbance of thyroid hormone-regulated genes. Ann N Y Acad Sci 1040: 454-6.

60. Dowling, P, O'Driscoll, L, O'Sullivan, F, Dowd, A, Henry, M, Jeppesen, PB et al., (2006) Proteomic screening of glucose-responsive and glucose non-responsive MIN-6 beta cells reveals differential expression of proteins involved in protein folding, secretion and oxidative stress. Proteomics 6: 6578-87.

61. Dhingra, V, Li, Q, Allison, AB, Stallknecht, DE and Fu, ZF, (2005) Proteomic profiling and neurodegeneration in west-nile-virus-infected neurons. J Biomed Biotechnol 2005: 271-9.

62. Metzner, C, Salmons, B, Gunzburg, WH, Gemeiner, M, Miller, I, Gesslbauer, B et al., (2006) MMTV accessory factor Naf affects cellular gene expression. Virology 346: 139-50.

63. Saito, S, Kusano, S, Koizuka, I and Nakashima, H, (2007) [The up-regulation of vimentin and ezrin in the Epstein-Barr virus LMP1 gene transfected cells]. Nippon Jibiinkoka Gakkai Kaiho 110: 24-31.

64. St-Louis, MC and Archambault, D, (2007) The equine arteritis virus induces apoptosis via caspase-8 and mitochondria-dependent caspase-9 activation. Virology 367: 147-55.

65. Gotoh, T, Terada, K, Oyadomari, S and Mori, M, (2004) hsp70-DnaJ chaperone pair prevents nitric oxide- and CHOP-induced apoptosis by inhibiting translocation of Bax to mitochondria. Cell Death Differ 11: 390-402.

66. Gutierrez-Escolano, AL, Vazquez-Ochoa, M, Escobar-Herrera, J and Hernandez-Acosta, J, (2003) La, PTB, and PAB proteins bind to the 3(') untranslated region of Norwalk virus genomic RNA. Biochem Biophys Res Commun 311: 759-66.

67. Kim, O, Park, M, Kang, H, Lim, S and Lee, CT, (2003) Differential protein expressions induced by adenovirus-mediated p16 gene transfer into Balb/c nude mouse. Proteomics 3: 2412-9.

68. Chang, LY, Ali, AR, Hassan, SS and AbuBakar, S, (2007) Human neuronal cell protein responses to Nipah virus infection. Virol J 4: 54.

69. Di Paolo, NC, Tuve, S, Ni, S, Hellstrom, KE, Hellstrom, I and Lieber, A, (2006) Effect of adenovirus-mediated heat shock protein expression and oncolysis in combination with low-dose cyclophosphamide treatment on antitumor immune responses. Cancer Res 66: 960-9.

70. Cassatella, MA, Huber, V, Calzetti, F, Margotto, D, Tamassia, N, Peri, G et al., (2006) Interferon-activated neutrophils store a TNF-related apoptosis-inducing ligand (TRAIL/Apo-2 ligand) intracellular pool that is readily mobilizable following exposure to proinflammatory mediators. J Leukoc Biol 79: 123-32.

71. Basu, S, Binder, RJ, Suto, R, Anderson, KM and Srivastava, PK, (2000) Necrotic but not apoptotic cell death releases heat shock proteins, which deliver a partial maturation signal to dendritic cells and activate the NF-kappa B pathway. Int Immunol 12: 1539-46.

72. Doss, MX, Winkler, J, Chen, S, Hippler-Altenburg, R, Sotiriadou, I, Halbach, M et al., (2007) Global transcriptome analysis of murine embryonic stem cell-derived cardiomyocytes. Genome Biol 8: R56.

73. Feng, P, Liang, C, Shin, YC, E, X, Zhang, W, Gravel, R et al., (2007) A Novel Inhibitory Mechanism of Mitochondrion-Dependent Apoptosis by a Herpesviral Protein. PLoS Pathog 3: e174.

74. Baines, CP, Kaiser, RA, Sheiko, T, Craigen, WJ and Molkentin, JD, (2007) Voltage-dependent anion channels are dispensable for mitochondrial-dependent cell death. Nat Cell Biol 9: 550-5.

75. Qiao, H and McMillan, JR, (2007) Gelsolin segment 5 inhibits HIV-induced T-cell apoptosis via Vpr-binding to VDAC. FEBS Lett 581: 535-40.

76. Malia, TJ and Wagner, G, (2007) NMR structural investigation of the mitochondrial outer membrane protein VDAC and its interaction with antiapoptotic Bcl-xL. Biochemistry 46: 514-25.

77. Tarze, A, Deniaud, A, Le Bras, M, Maillier, E, Molle, D, Larochette, N et al., (2007) GAPDH, a novel regulator of the pro-apoptotic mitochondrial membrane permeabilization. Oncogene 26: 2606-20.

78. Abu-Hamad, S, Zaid, H, Israelson, A, Nahon, E and Shoshan-Barmatz, V, (2008) Hexokinase -I protection against apoptotic cell death is mediated via interaction with the voltage-dependent anion channel-1: Mapping the site of binding. J Biol Chem.

79. Zhan, XA, Wang, M, Xu, ZR, Li, WF and Li, JX, (2006) Evaluation of caspase-dependent apoptosis during fluoride-induced liver lesion in pigs. Arch Toxicol 80: 74-80.

80. Sun, F, Hamagawa, E, Tsutsui, C, Sakaguchi, N, Kakuta, Y, Tokumaru, S et al., (2003) Evaluation of oxidative stress during apoptosis and necrosis caused by D-galactosamine in rat liver. Biochem Pharmacol 65: 101-7.

81. Hayami, S, Ikeda, K, Sun, F, Tanaka, K and Kojo, S, (1999) Increase of caspase-3 activity in rat liver and plasma by thioacetamide. Biochem Pharmacol 58: 1941-3.

82. Moseley, P, (2000) Stress proteins and the immune response. Immunopharmacology 48: 299-302.

83. Poland, J, Sinha, P, Siegert, A, Schnolzer, M, Korf, U and Hauptmann, S, (2002) Comparison of protein expression profiles between monolayer and spheroid cell culture of HT-29 cells revealed fragmentation of CK18 in three-dimensional cell culture. Electrophoresis 23: 1174-84.

84. Aisaki, K, Kanno, H, Oyaizu, N, Hara, Y, Miwa, S and Ikawa, Y, (1999) Apoptotic changes precede mitochondrial dysfunction in red cell-type pyruvate kinase mutant mouse erythroleukemia cell lines. Jpn J Cancer Res 90: 171-9.

85. Ruddat, VC, Whitman, S, Klein, RD, Fischer, SM and Holman, TR, (2005) Evidence for downregulation of calcium signaling proteins in advanced mouse adenocarcinoma. Prostate 64: 128-38.

86. Ma, C, Guan, SH, Yang, M, Liu, X and Guo, DA, (2008) Differential protein expression in mouse splenic mononuclear cells treated with polysaccharides from spores of Ganoderma lucidum. Phytomedicine.

87. Chau, YP, Shiah, SG, Don, MJ and Kuo, ML, (1998) Involvement of hydrogen peroxide in topoisomerase inhibitor beta-lapachone-induced apoptosis and differentiation in human leukemia cells. Free Radic Biol Med 24: 660-70.

88. Nishimura, K, Ueda, K, Guwanan, E, Sakakibara, S, Do, E, Osaki, E et al., (2004) A posttranscriptional regulator of Kaposi's sarcoma-associated herpesvirus interacts with RNA-binding protein PCBP1 and controls gene expression through the IRES. Virology 325: 364-78.

89. Lewis, SM, Veyrier, A, Hosszu Ungureanu, N, Bonnal, S, Vagner, S and Holcik, M, (2007) Subcellular relocalization of a trans-acting factor regulates XIAP IRES-dependent translation. Mol Biol Cell 18: 1302-11.

90. Kim, JH, Paek, KY, Choi, K, Kim, TD, Hahm, B, Kim, KT et al., (2003) Heterogeneous nuclear ribonucleoprotein C modulates translation of c-myc mRNA in a cell cycle phase-dependent manner. Mol Cell Biol 23: 708-20.

91. Holcik, M and Korneluk, RG, (2000) Functional characterization of the X-linked inhibitor of apoptosis (XIAP) internal ribosome entry site element: role of La autoantigen in XIAP translation. Mol Cell Biol 20: 4648-57.

92. Holcik, M, Gordon, BW and Korneluk, RG, (2003) The internal ribosome entry site-mediated translation of antiapoptotic protein XIAP is modulated by the heterogeneous nuclear ribonucleoproteins C1 and C2. Mol Cell Biol 23: 280-8.

93. Sung, FL, Pang, RT, Ma, BB, Lee, MM, Chow, SM, Poon, TC et al., (2006) Pharmacoproteomics study of cetuximab in nasopharyngeal carcinoma. J Proteome Res 5: 3260-7.

94. Nahlik, KW, Mleczko, AK, Gawlik, MK and Rokita, HB, (2003) Modulation of GAPDH expression and cellular localization after vaccinia virus infection of human adherent monocytes. Acta Biochim Pol 50: 667-76.

95. Brown, VM, Krynetski, EY, Krynetskaia, NF, Grieger, D, Mukatira, ST, Murti, KG et al., (2004) A novel CRM1-mediated nuclear export signal governs nuclear accumulation of glyceraldehyde-3-phosphate dehydrogenase following genotoxic stress. J Biol Chem 279: 5984-92.

96. Zhang, B, Zhang, Y, Dagher, MC and Shacter, E, (2005) Rho GDP dissociation inhibitor protects cancer cells against drug-induced apoptosis. Cancer Res 65: 6054-62.

97. Krieser, RJ and Eastman, A, (1999) Cleavage and nuclear translocation of the caspase 3 substrate Rho GDP-dissociation inhibitor, D4-GDI, during apoptosis. Cell Death Differ 6: 412-9.

98. Waterhouse, NJ, Oliaro, J and Pinkoski, MJ, (2006) A 'polarized' look at alpha-tubulin cleavage by granzyme B. Cell Death Differ 13: 1839-41.

99. Lindsay, ME, Plafker, K, Smith, AE, Clurman, BE and Macara, IG, (2002) Npap60/Nup50 is a tri-stable switch that stimulates importin-alpha:beta-mediated nuclear protein import. Cell 110: 349-60.

100. Galati, D, Paiardini, M, Cervasi, B, Albrecht, H, Bocchino, M, Costantini, A et al., (2003) Specific changes in the posttranslational regulation of nucleolin in lymphocytes from patients infected with human immunodeficiency virus. J Infect Dis 188: 1483-91.

101. Xie, M, Kobayashi, I, Kiyoshima, T, Yamaza, H, Honda, JY, Takahashi, K et al., (2007) Functional implication of nucleolin in the mouse first molar development. J Biol Chem 282: 23275-83.

102. Corcoran, CA, Huang, Y and Sheikh, MS, (2006) The regulation of energy generating metabolic pathways by p53. Cancer Biol Ther 5: 1610-3.

103. Widlak, W, Benedyk, K, Vydra, N, Glowala, M, Scieglinska, D, Malusecka, E et al., (2003) Expression of a constitutively active mutant of heat shock factor 1 under the control of testis-specific hst70 gene promoter in transgenic mice induces degeneration of seminiferous epithelium. Acta Biochim Pol 50: 535-41.

104. Widlak, W, (2006) [The heat shock response and HSP70 gene expression in male germ cells]. Postepy Biochem 52: 289-95.

105. Averill-Bates, DA, Ke, Q, Tanel, A, Roy, J, Fortier, G and Agostinelli, E, (2008) Mechanism of cell death induced by spermine and amine oxidase in mouse melanoma cells. Int J Oncol 32: 79-88.

106. Schiller, M, Blank, N, Heyder, P, Herrmann, M, Gaipl, US, Kalden, JR et al., (2005) Induction of apoptosis by spermine-metabolites in primary human blood cells and various tumor cell lines. Apoptosis 10: 1151-62.

107. Berry, DA, Keogh, A and dos Remedios, CG, (2001) Nuclear membrane proteins in failing human dilated cardiomyopathy. Proteomics 1: 1507-12.

108. Wang, J, Belcher, JD, Marker, PH, Wilcken, DE, Vercellotti, GM and Wang, XL, (2001) Cytomegalovirus inhibits p53 nuclear localization signal function. J Mol Med 78: 642-7.

109. Cui, XS and Kim, NH, (2005) Polyamines inhibit apoptosis in porcine parthenotes developing in vitro. Mol Reprod Dev 70: 471-7.

110. Yanagawa, T, Funasaka, T, Tsutsumi, S, Watanabe, H and Raz, A, (2004) Novel roles of the autocrine motility factor/phosphoglucose isomerase in tumor malignancy. Endocr Relat Cancer 11: 749-59.

111. Hashimoto, M, Inoue, S, Ogawa, S, Conrad, C, Muramatsu, M, Shackelford, D et al., (1998) Rapid fragmentation of vimentin in human skin fibroblasts exposed to tamoxifen: a possible involvement of caspase-3. Biochem Biophys Res Commun 247: 401-6.

112. Morishima, N, (1999) Changes in nuclear morphology during apoptosis correlate with vimentin cleavage by different caspases located either upstream or downstream of Bcl-2 action. Genes Cells 4: 401-14.

113. Slee, EA, Adrain, C and Martin, SJ, (2001) Executioner caspase-3, -6, and -7 perform distinct, non-redundant roles during the demolition phase of apoptosis. J Biol Chem 276: 7320-6.

114. Byun, Y, Chen, F, Chang, R, Trivedi, M, Green, KJ and Cryns, VL, (2001) Caspase cleavage of vimentin disrupts intermediate filaments and promotes apoptosis. Cell Death Differ 8: 443-50.

115. Lai, MY, Hour, MJ, Wing-Cheung Leung, H, Yang, WH and Lee, HZ, (2007) Chaperones are the target in aloe-emodin-induced human lung nonsmall carcinoma H460 cell apoptosis. Eur J Pharmacol 573: 1-10.

116. Acarin, L, Villapol, S, Faiz, M, Rohn, TT, Castellano, B and Gonzalez, B, (2007) Caspase-3 activation in astrocytes following postnatal excitotoxic damage correlates with cytoskeletal remodeling but not with cell death or proliferation. Glia 55: 954-65.

117. Wolter, KG, Hsu, YT, Smith, CL, Nechushtan, A, Xi, XG and Youle, RJ, (1997) Movement of Bax from the cytosol to mitochondria during apoptosis. J Cell Biol 139: 1281-92.

118. Grzanka, A, Grzanka, D and Orlikowska, M, (2003) Cytoskeletal reorganization during process of apoptosis induced by cytostatic drugs in K-562 and HL-60 leukemia cell lines. Biochem Pharmacol 66: 1611-7.

119. Stefanovic, S, Windsor, M, Nagata, KI, Inagaki, M and Wileman, T, (2005) Vimentin rearrangement during African swine fever virus infection involves retrograde transport along microtubules and phosphorylation of vimentin by calcium calmodulin kinase II. J Virol 79: 11766-75.

120. Yang, Y and Loscalzo, J, (2005) S-nitrosoprotein formation and localization in endothelial cells. Proc Natl Acad Sci U S A 102: 117-22.

121. Lin, KI, Pasinelli, P, Brown, RH, Hardwick, JM and Ratan, RR, (1999) Decreased intracellular superoxide levels activate Sindbis virus-induced apoptosis. J Biol Chem 274: 13650-5.

122. Kotamraju, S, Chitambar, CR, Kalivendi, SV, Joseph, J and Kalyanaraman, B, (2002) Transferrin receptor-dependent iron uptake is responsible for doxorubicin-mediated apoptosis in endothelial cells: role of oxidant-induced iron signaling in apoptosis. J Biol Chem 277: 17179-87.

123. Kim, HS and Lee, MS, (2005) Essential role of STAT1 in caspase-independent cell death of activated macrophages through the p38 mitogen-activated protein kinase/STAT1/reactive oxygen species pathway. Mol Cell Biol 25: 6821-33.

124. Martinet, W, Schrijvers, DM, Herman, AG and De Meyer, GR, (2006) z-VAD-fmk-induced non-apoptotic cell death of macrophages: possibilities and limitations for atherosclerotic plaque stabilization. Autophagy 2: 312-4.

125. Lee, HJ, Oh, YK, Rhee, M, Lim, JY, Hwang, JY, Park, YS et al., (2007) The role of STAT1/IRF-1 on synergistic ROS production and loss of mitochondrial transmembrane potential during hepatic cell death induced by LPS/d-GalN. J Mol Biol 369: 967-84.

126. Almeida, B, Buttner, S, Ohlmeier, S, Silva, A, Mesquita, A, Sampaio-Marques, B et al., (2007) NO-mediated apoptosis in yeast. J Cell Sci 120: 3279-88.

127. Miura, M, Zhu, H, Rotello, R, Hartwieg, EA and Yuan, J, (1993) Induction of apoptosis in fibroblasts by IL-1 beta-converting enzyme, a mammalian homolog of the C. elegans cell death gene ced-3. Cell 75: 653-60.

128. Cossarizza, A, (2008) Apoptosis and HIV infection: about molecules and genes. Curr Pharm Des 14: 237-44.

129. Lomonosova, E, Subramanian, T and Chinnadurai, G, (2002) Requirement of BAX for efficient adenovirus-induced apoptosis. J Virol 76: 11283-90.

130. Fischer, R, Baumert, T and Blum, HE, (2007) Hepatitis C virus infection and apoptosis. World J Gastroenterol 13: 4865-72.

131. Yamasaki, H and Irie, H, (2006) [HSV infection and apoptosis]. Nippon Rinsho 64 Suppl 3: 167-70.

132. Garnett, TO and Duerksen-Hughes, PJ, (2006) Modulation of apoptosis by human papillomavirus (HPV) oncoproteins. Arch Virol 151: 2321-35.

133. Ludwig, S, Pleschka, S, Planz, O and Wolff, T, (2006) Ringing the alarm bells: signalling and apoptosis in influenza virus infected cells. Cell Microbiol 8: 375-86.

134. Roberts, LO, Al-Molawi, N, Carter, MJ and Kass, GE, (2003) Apoptosis in cultured cells infected with feline calicivirus. Ann N Y Acad Sci 1010: 587-90.

135. Al-Molawi, N, Beardmore, VA, Carter, MJ, Kass, GE and Roberts, LO, (2003) Caspase-mediated cleavage of the feline calicivirus capsid protein. J Gen Virol 84: 1237-44.

136. Pozarowski, P, Huang, X, Halicka, DH, Lee, B, Johnson, G and Darzynkiewicz, Z, (2003) Interactions of fluorochrome-labeled caspase inhibitors with apoptotic cells: a caution in data interpretation. Cytometry A 55: 50-60.

137. Rozman-Pungercar, J, Kopitar-Jerala, N, Bogyo, M, Turk, D, Vasiljeva, O, Stefe, I et al., (2003) Inhibition of papain-like cysteine proteases and legumain by caspase-specific inhibitors: when reaction mechanism is more important than specificity. Cell Death Differ 10: 881-8.

138. Chauvier, D, Ankri, S, Charriaut-Marlangue, C, Casimir, R and Jacotot, E, (2007) Broad-spectrum caspase inhibitors: from myth to reality? Cell Death Differ 14: 387-91.

139. Shun-mei, E, Xiao, WM, Wang, KK, Wang, QP, Liu, MD, Liu, K et al., (2006) [HSF1 inhibits heat stress-induced apoptosis in Raw264.7 macrophages]. Zhong Nan Da Xue Xue Bao Yi Xue Ban 31: 162-6.

140. Pelfrey, CM, Tranquill, LR, Boehme, SA, McFarland, HF and Lenardo, MJ, (1995) Two mechanisms of antigen-specific apoptosis of myelin basic protein (MBP)-specific T lymphocytes derived from multiple sclerosis patients and normal individuals. J Immunol 154: 6191-202.

141. Ramamoorthy, L and Tizard, IR, (1998) Induction of apoptosis in a macrophage cell line RAW 264.7 by acemannan, a beta-(1,4)-acetylated mannan. Mol Pharmacol 53: 415-21.

142. Chin, YE, Kitagawa, M, Kuida, K, Flavell, RA and Fu, XY, (1997) Activation of the STAT signaling pathway can cause expression of caspase 1 and apoptosis. Mol Cell Biol 17: 5328-37.

143. Kumar, A, Commane, M, Flickinger, TW, Horvath, CM and Stark, GR, (1997) Defective TNF-alpha-induced apoptosis in STAT1-null cells due to low constitutive levels of caspases. Science 278: 1630-2.

APPENDICES

APPENDIX A

NON-CONTRAST IMAGES OF INFECTED AND NON-INFECTED CELLS

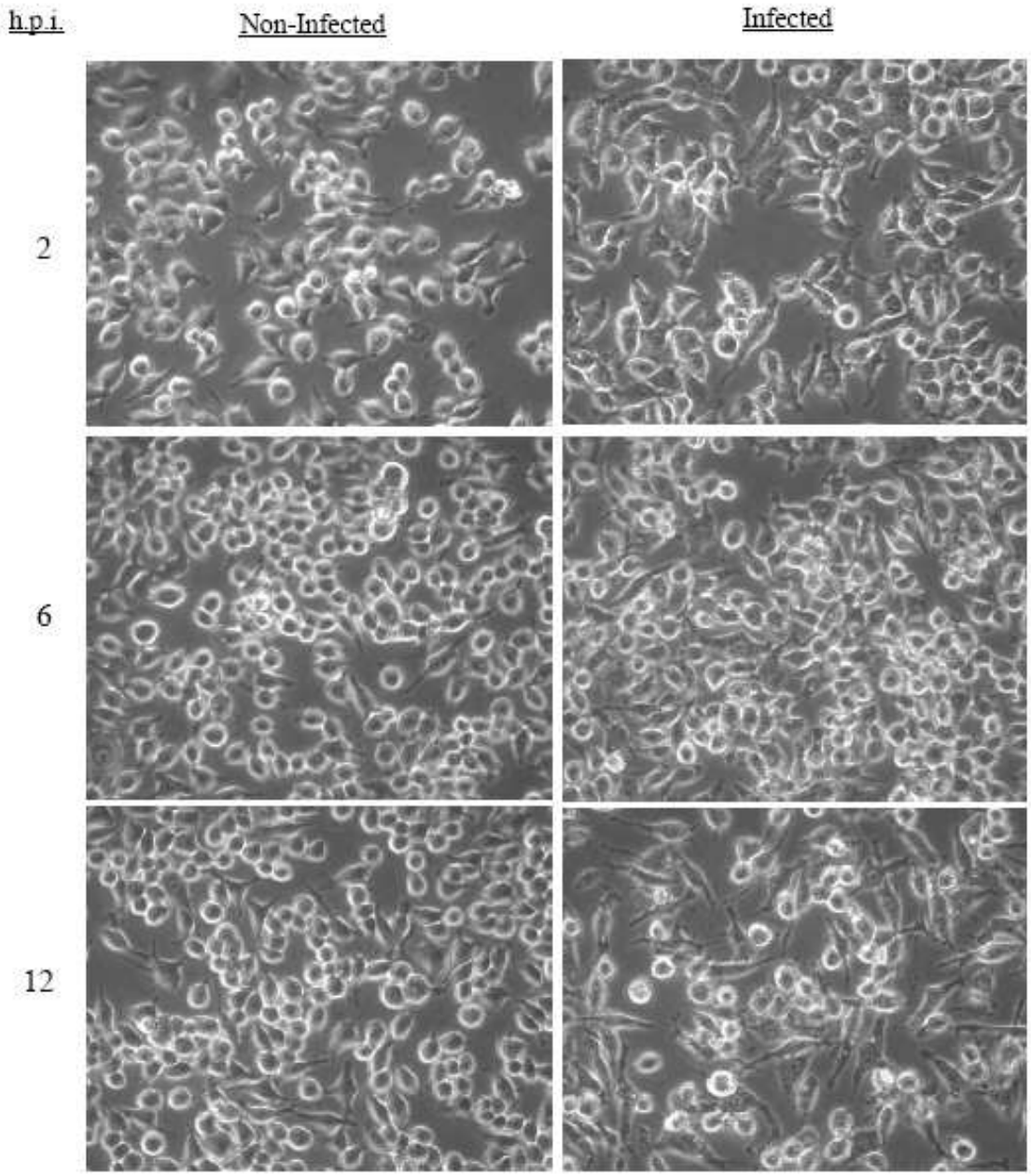

Appendix A. Non-contrast images of infected and non-infected cells adhered to a cell culture well. Samples were taken at 2, 6, and 12 h.p.i.

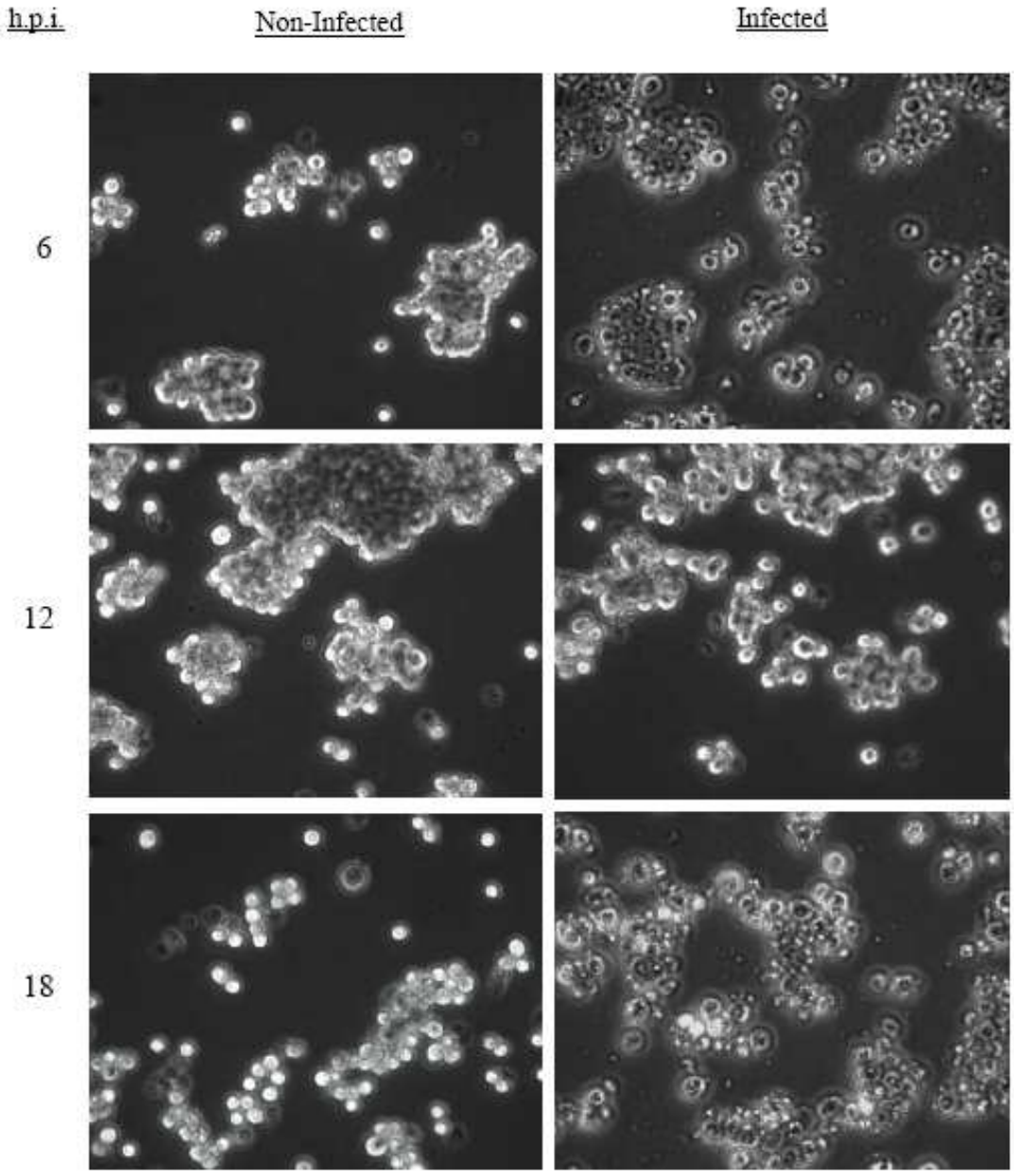

Appendix A continued. Non-contrast images of infected and non-infected cells on a glass slide at 6, 12, and 18 h.p.i.. Cells were scraped, harvested, pelleted, washed, and re-suspended in PBS.

APPENDIX B

FLUORESCENT IMAGES OF HOECHST STAINING IN INFECTED AND NON-INFECTED CELLS

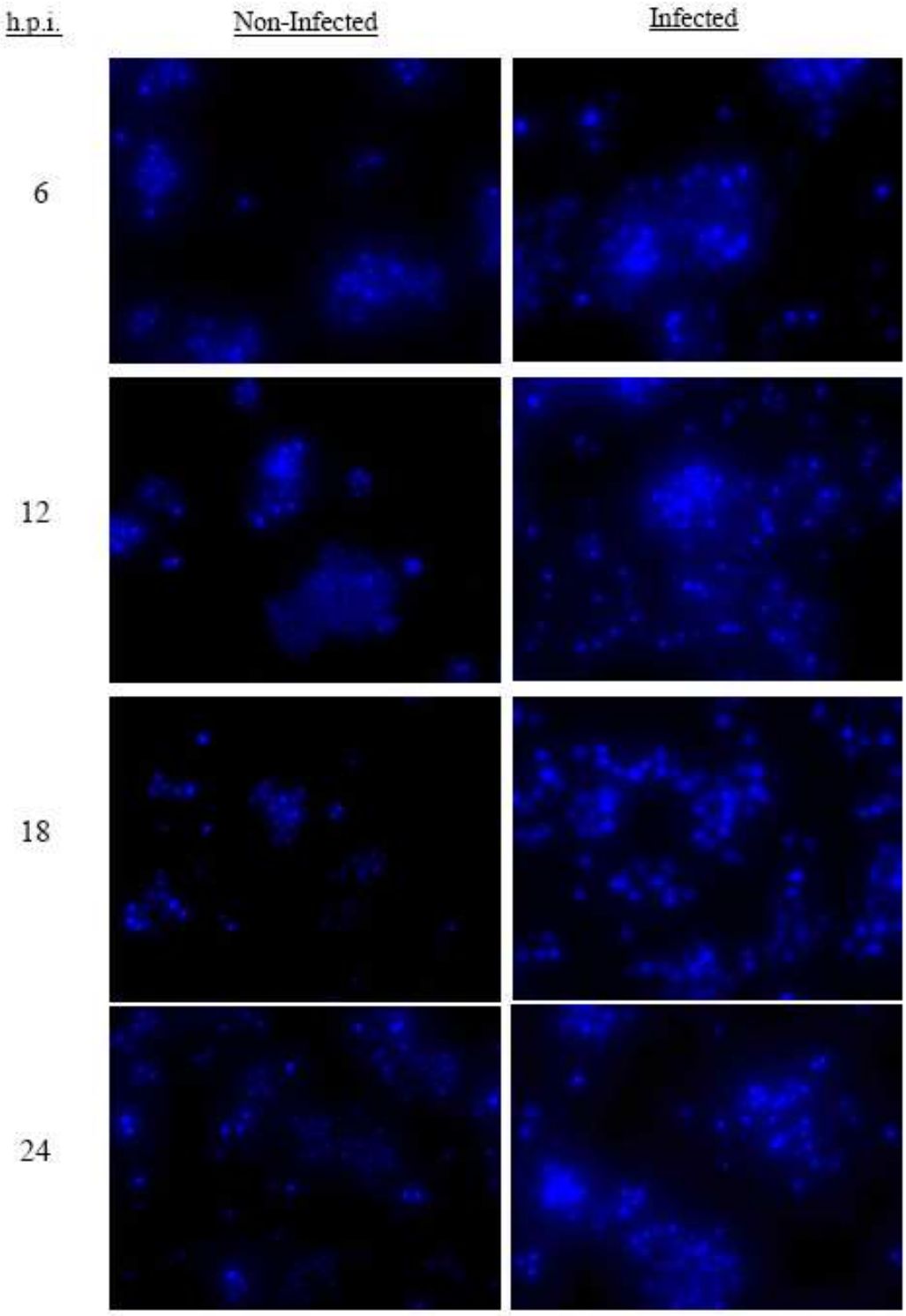

Appendix B. Florescent images of infected and non-infected cells stained with Hoechst stain. Brightly stained spots show chromatin condensation, a sign of apoptosis.

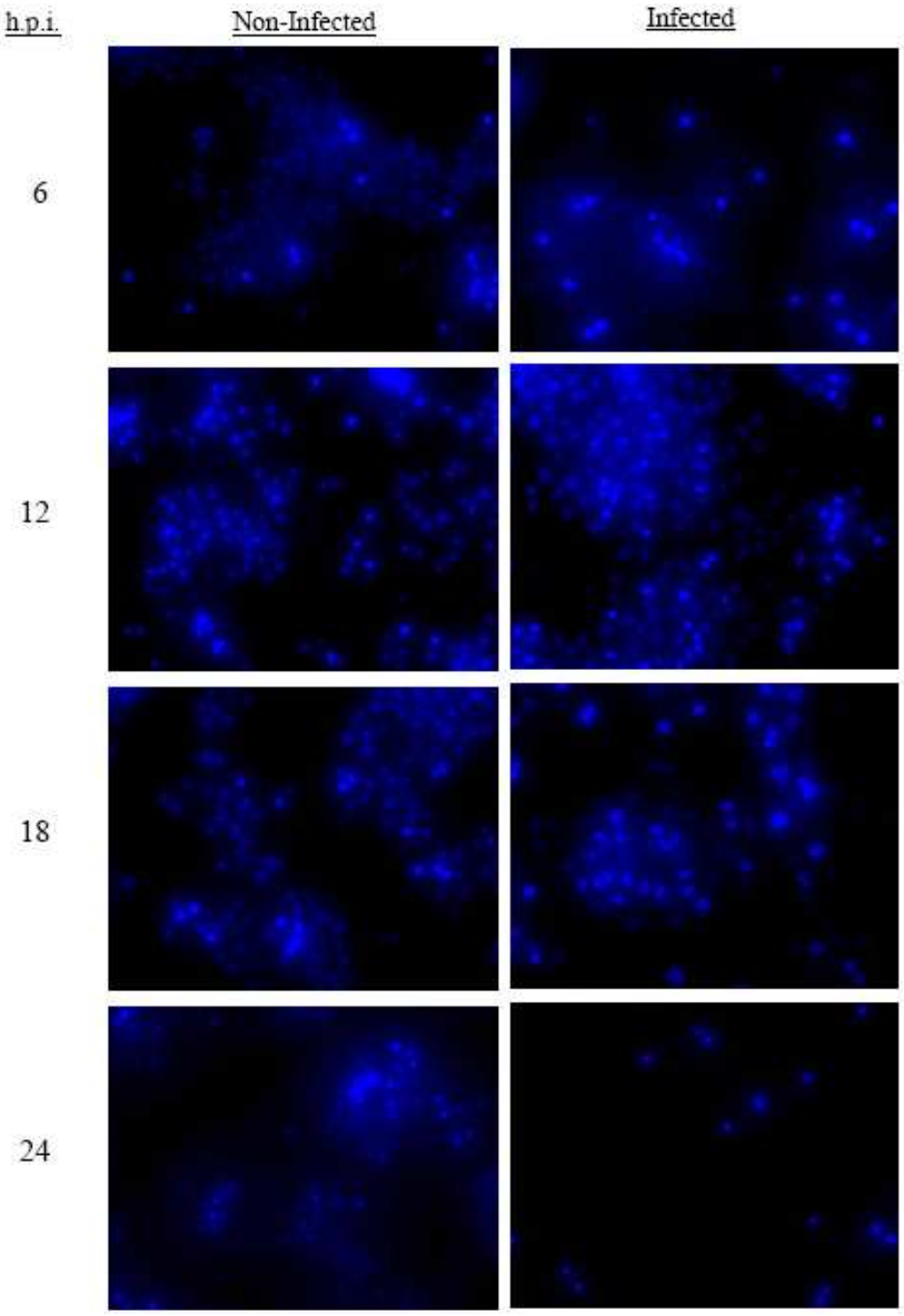

Appendix B continued. Florescent images of infected and non-infected cells in the presence of a pan-caspase inhibitor stained with Hoechst stain.

APPENDIX C

FLUORESCENT IMAGES OF PROPIDIUM IODIDE STAINING IN INFECTED AND NON-INFECTED CELLS

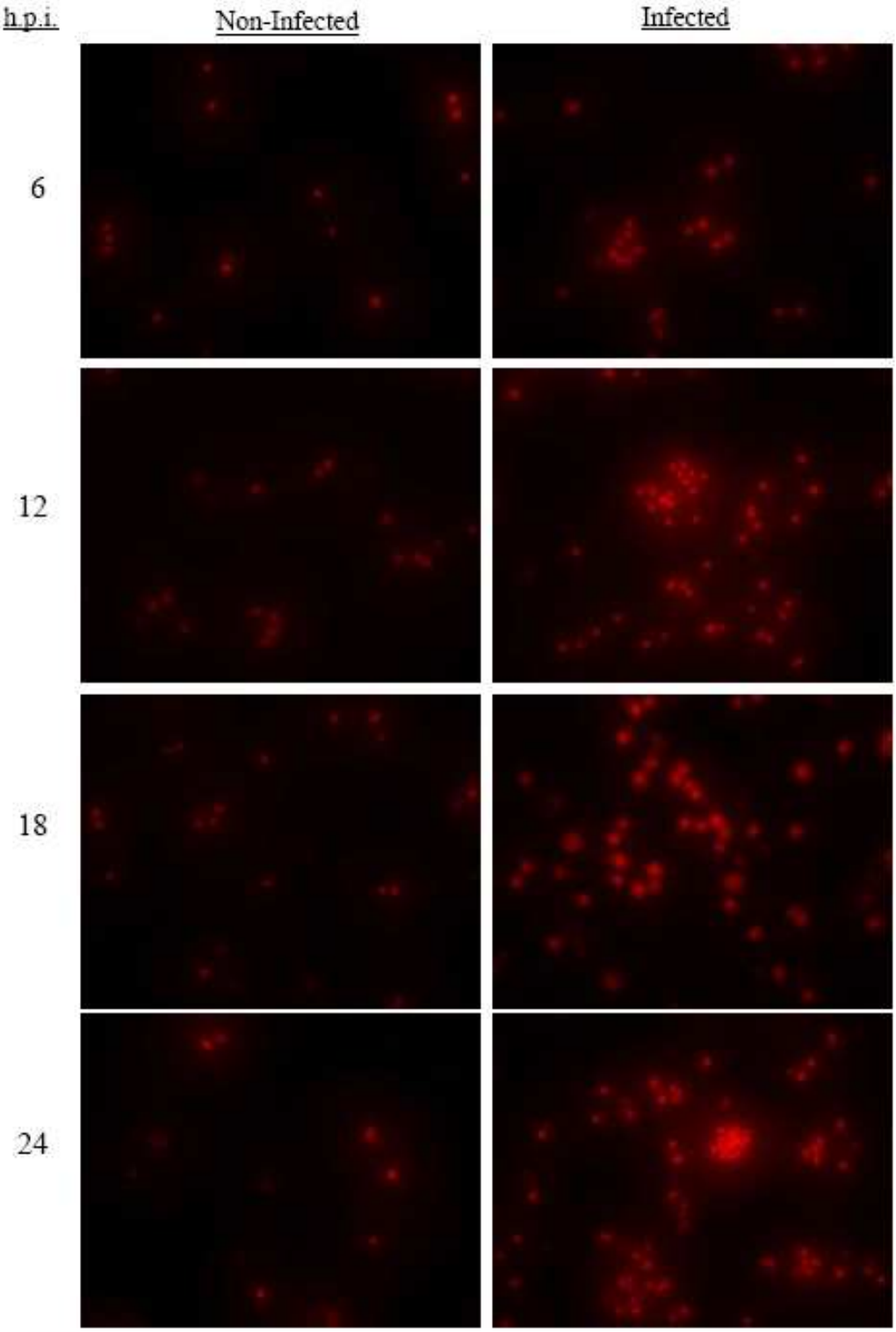

Appendix C. Florescent images of infected and non-infected cells stained with propidium iodide stain. Brightly stained spots show membrane permeability.

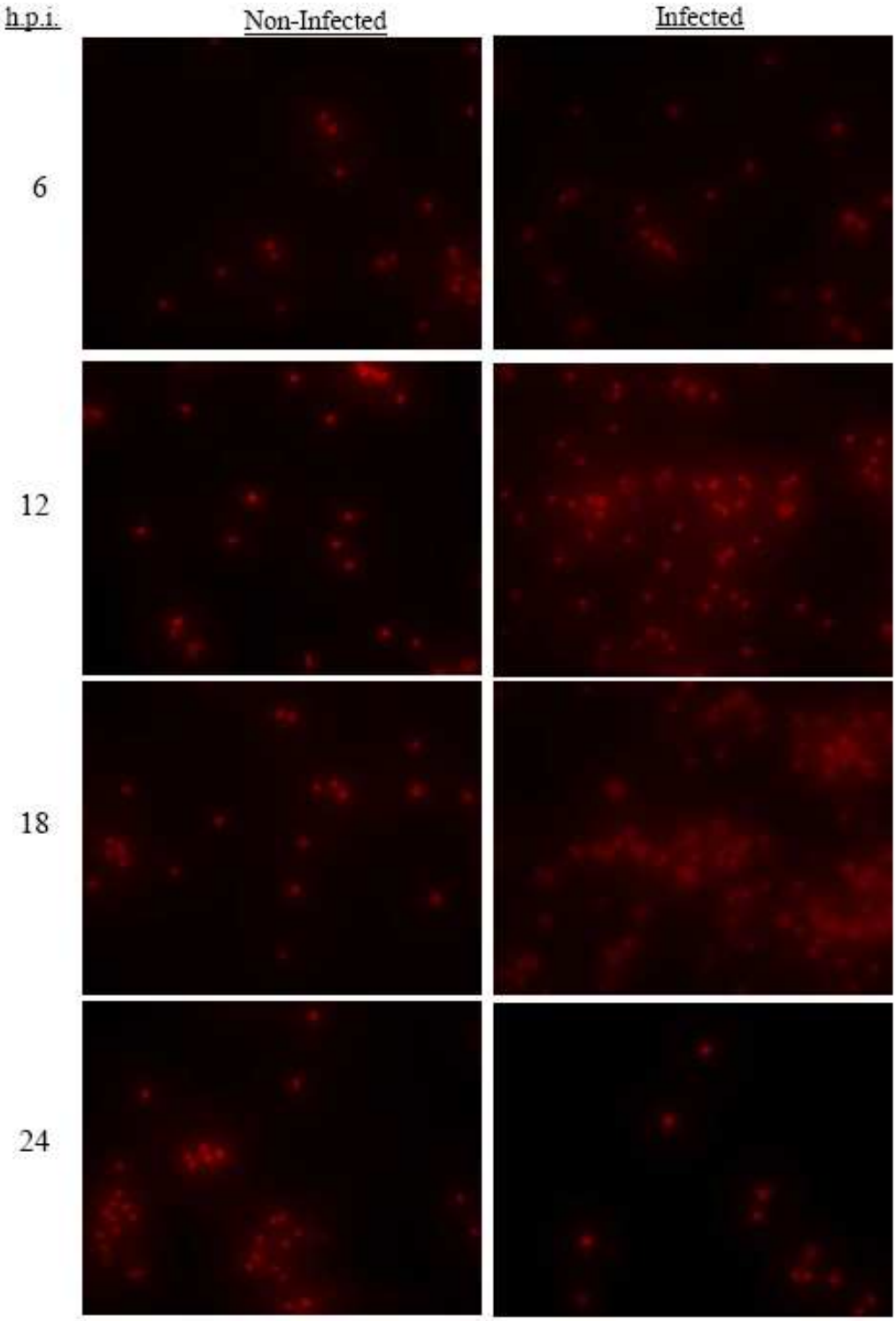

Appendix C continued. Florescent images of infected and non-infected cells in the presence of a pan-caspase inhibitor stained with propidium iodide stain.